This thesis, having been approved by the special Faculty Committee, is accepted by the Graduate School of the University of Wyoming in partial fulfillment of the requirements for the degree of

Master of Science

R. J. McCulloch
Dean of the Graduate School

Date November 11, 1975

A CLOUD FREE VAULT

John F. Weaver

A Thesis

Submitted to the

Department of Atmospheric Science and

the Graduate School of the University of Wyoming

in Partial Fulfillment of Requirements

for the Degree of

Master of Science

University of Wyoming

Laramie, Wyoming

December 1975

Weaver, John F., A Cloud Free Vault, M.S., Department of Atmospheric Science, October, 1975.

A severe squall line, with several isolated storms near its southernmost end, was observed near Grover, Colorado, on the afternoon of 22 July 73 by the NHRE storm monitoring system. The northern segment of the squall line was oriented parallel to cloud level winds (i.e., northeast-southwest), while the southern segment was aligned north-south. The northern segment developed an extensive cloud free vault intruding into the cloud base above the lifting condensation level (LCL) between the precipitation and the updraft pedestal. No downdraft or gust front was observed from the northern segment. Downdrafts and a gust front characterized by a pressure jump of +3 mb and peak winds of 60 knots were produced by both the southern segment and the isolated storms.

Examination of thermodynamic state parameters obtained by aircraft, mesonetwork stations and rawinsondes show that the occurrence of the cloud free vault was a result of (1) minimized entrainment due to the orientation of the squall line with respect to the cloud level winds and (2) a consequent failure of the outflow to gain the density differential required to overcome the momentum of the inflow and thereby initiate a gust front.

ACKNOWLEDGMENTS

Data used in this thesis were gathered as a part of the Department of Atmospheric Science, University of Wyoming's participation in the National Hail Research Experiment (NHRE). The NHRE is sponsored by the National Science Foundation (NSF).

My deepest appreciation goes to the faculty and staff of the Department of Atmospheric Science (University of Wyoming), but especially to my advisor, Dr. John D. Marwitz, for his assistance in the preparation of this thesis and his patient guidance throughout my graduate studies.

I wish also to express my gratitude to Dr. Robert J. Lavigne for his helpful comments concerning the grammatical composition of this paper.

TABLE OF CONTENTS

LIST OF FIGURES

Figure | Page

Figure — Page

CHAPTER I

LITERATURE REVIEW

1.1 Introduction

Although the thunderstorm, and the processes initiating it, have fascinated mankind for thousands of years, its resultant inner structure has remained a mystery until quite recently. Earliest explanations for the phenomenon commonly appeared in mythology, while more logical notions were offered by early scholars (e.g., see Aristotle's Meteorologica, as discussed by Lee, 1962). Unfortunately, most early interpretations of thunderstorm related events were incorrect. Perhaps because the thunderstorm develops high above the earth's surface--beyond man's natural reach--few notable advances toward understanding the phenomenon were made prior to the late 19th Century.

Late 19th and early 20th Century interpretations of thunderstorm structure were based primarily on visual observation. However, the renewed interest in science which came with the Renaissance had given man a deeper understanding of natural forces. More reasonable explanations of thunderstorm processes were thus offered by scientists of the time. A rather extensive review of thunderstorm models conceived during this period can be found in Ludlam (1963). In his treatment, Ludlam notes that many of these ideas (notably those concerning the distribution of airflow and precipitation in thunderstorms) were correct in

essential details. However, the validity of these early conceptions lacked experimental verification.

With the discovery and improvement of radar and the equipping of aircraft with instrumentation, more sophisticated research was possible. Data thus collected provided atmospheric scientists with a means of constructing dynamical models to explain the structural features of the thunderstorm.

The analysis contained herein deals with a previously unexplained structural feature--the cloud free vault. This term was coined to describe a volume of cloud-free air intruding into cloud base, above the lifting condensation level (LCL), between the updraft pedestal and the precipitation curtain. There is a similar structure occasionally observed to occur ahead of the updraft pedestal which contains strong updrafts (see e.g., Browning and Foote, 1975). These two different phenomena should not be confused.

The objective of the present study is to examine the available thermodynamic and kinematic data in an attempt to explain the presence of the visual cloud free vault, as well as establish its origin and importance.

Much of the data for the present study were gathered by radar systems and instrumented aircraft and the conclusions rely heavily upon kinematic models of thunderstorm structure developed by investigators (see below) utilizing these relatively new tools. Consequently, it is appropriate to present here a review of the evolution of thought regarding the thunderstorm.

1.2 General Thunderstorm Structure

The first published data utilizing the new capabilities for thunderstorm research resulted from the United States Weather Bureau's Thunderstorm Project (1946-1947) in Florida and Ohio. A report emerged entitled, "Thunderstorm Structure and Circulation," by Byers and Braham (1948), which outlined the major findings of this project. The results provided experimental verification for some points, quantified certain features, furnished deeper insights into others, and suggested new directions for research.

There were two particular results from this research relevant to the material presented in this thesis. The data showed that a thunderstorm most often consists of isolated regions of convective activity which were termed "cells." These cells are often found imbedded in non-convective cloud material. The individual cells exhibit a three-stage life cycle consisting of:

1. "Cumulus stage," characterized by updrafts throughout the forming cloud.
2. "Mature stage," characterized by a continuation of updrafts and development of cool air downdrafts (with the onset of precipitation).
3. "Dissipating stage," characterized by a dissipating updraft and a spreading of the downdraft beneath the cell, with the tendency being for the outflow to spread preferentially to one side of the cell. During this stage the air mass discontinuity between the environment and the outflow acts as a

miniature cold front which often plays an important role in initiating new cells via mechanical lifting.

The second significant result, with respect to the study, was that entrainment (i.e., the drawing in of external air) and the consequent mixing of environmental air with that of the thunderstorm modified the storm appreciably. One effect of entrainment is to cool the updraft--both by mixing with cooler mid-level air and by evaporating cloud particles as they pass through this intruding drier air. The result is that the updraft lapse rate becomes somewhat steeper than moist-adiabatic. Entrainment was also postulated to affect the downdraft by furnishing a non-adiabatic cooling mechanism through which the downdraft (triggered and maintained by falling raindrops) might be assisted.

This pioneering work, coupled with subsequent experiments and more recently evolved models, has been summarized by Ludlam (1963). Of perhaps greater importance is that within the paper presented by Ludlam (1963) was outlined a comprehensive case study of a storm which occurred near Wokingham, England, on 9 July 1959 (analyzed by Browning and Ludlam, 1962). The study concerned a type of storm previously uninvestigated, i.e., the large, long-lived, single cell, steady-state thunderstorm termed a "supercell" (Browning, 1962). On the basis of the Wokingham storm, a supercell model was postulated from several distinctive radar features, as well as supportive surface observations of wind and precipitation.

The most important radar feature observed by Browning and Ludlam (1962) was a region intruding vertically into the radar image on the forward edge of the storm in which there was no detectable echo (Figure 1.1). This region, designated the echo-free vault (not related to the cloud free vault), was bounded by a vertical precipitation "wall" on the central and right-hand portion of the front of the storm. Further, the echo-free vault was capped by a "forward overhang" of the radar echo.

Synthesis of radar data with surface meteorological data resulted in the supercell model illustrated in Figure 1.2. This diagram, portraying the proposed air parcel trajectories relative to storm motion, shows: (1) the updraft entering the storm on the right front flank (beneath the overhang), (2) a micro-scale cold front at the inflow-outflow boundary on the right front edge of the storm, and (3) air entraining into the storm at mid-levels.

In addition to the kinematic features of the supercell illustrated by this model, Ludlam (1963) outlined still another important conclusion reached by Browning and Ludlam (1962). Up to the time of the Wokingham storm analysis, large vertical wind shears were assumed to inhibit convective growth. However, some accumulated evidence existed to indicate that strong horizontal intrusion of mid-level air occurred during some of the more severe thunderstorms. As Ludlam notes, some storms had been analyzed in which wet-bulb potential temperature (θ_w) values behind the micro-scale cold front frequently corresponded to values encountered at heights of several kilometers. The implica-

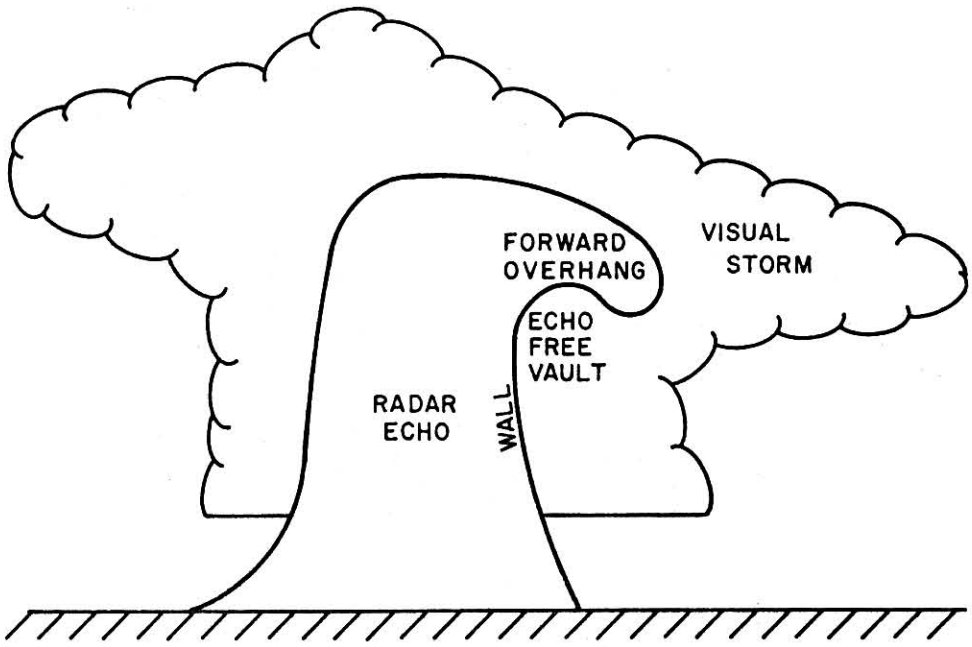

Figure 1.1 A schematic interpretation of the radar and visual structure of the Wokingham supercell storm.

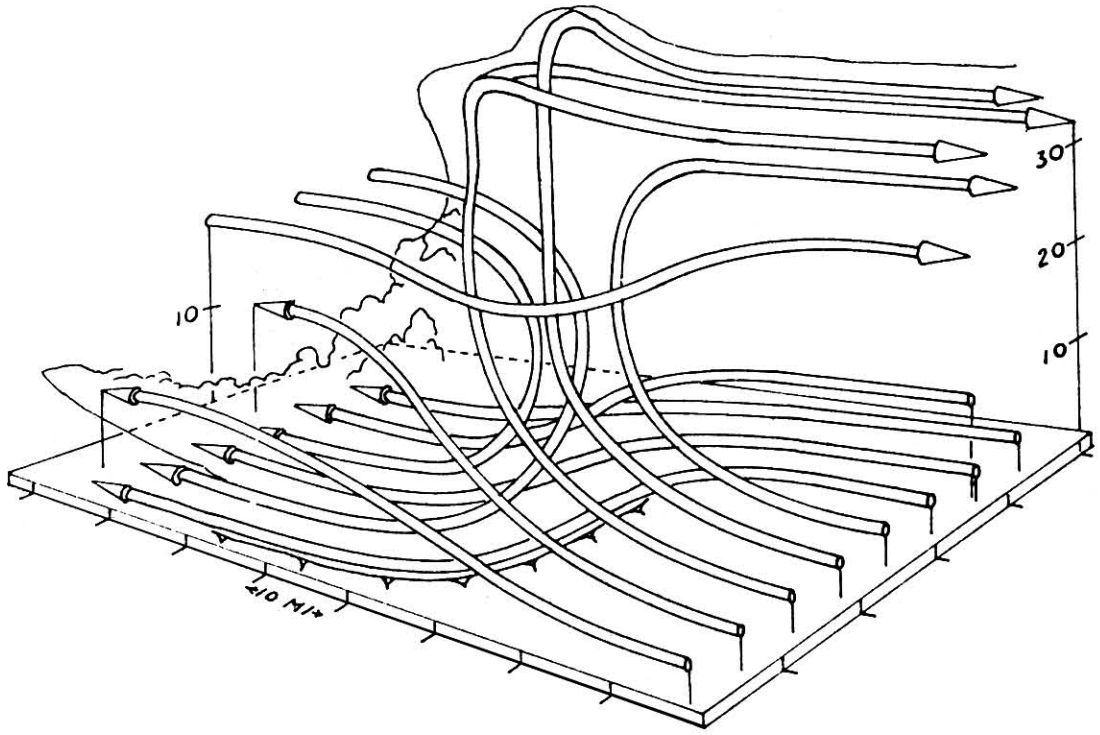

Figure 1.2 Three-dimensional model of the airflow within the Wokingham storm (after Browning and Ludlam, 1962).

tion from this discovery was that at least some of the air appearing in the surface outflow had been mid-level, environmental air which had been transported downward.

Ludlam (1963) argued that without wind shear, an updraft necessarily forms upright. As condensation occurs, precipitation falls through the updraft, either impeding its growth or destroying it completely. However, in the presence of wind shear the updraft may become tilted and separate from the downdraft. Such structuring would create a quasi-steady, updraft-downdraft system working side by side without mutual interference.

Furthermore, in the presence of shear, mid-level air might intrude into the storm. Ludlam points out that early investigators (e.g., Normand, 1938) had suggested that if water droplets could be evaporated into already cool entraining air, the kinetic energy of the downdraft might be substantially increased by a decrease in buoyancy and the consequent gravitational sinking. It would appear from these arguments that vertical wind shear is an extremely important (possibly even necessary) condition for the occurrence of severe local storms.

The basic supercell model proposed by Browning and Ludlam (1962) has not been appreciably altered by succeeding investigators. A subsequent study by Browning and Donaldson (1963) analyzed a supercell storm which occurred near Geary, Oklahoma, on 4 May 1961. Both were similar to those of the Wokingham storm. The Geary storm synthesis thus served to confirm the results obtained by Browning and Ludlam (1962).

Subsequent investigations further confirmed the model suggested by Browning and Ludlam (1962). On 28 July 1969, Marwitz and Berry (1971) in Alberta, Canada, conducted a flight into a weak echo region (WER*) to verify that this region inside the storm was indeed an updraft zone as suggested by Browning and Ludlam (1962). Several other investigators had already observed an organized updraft zone beneath this portion of the cloud (e.g., Marwitz et al., 1969; Auer et al., 1970). Results from the Marwitz and Berry experiment confirmed that an updraft zone existed within this WER.

Thus, the principal features of the air circulation within large, well organized thunderstorms were generally established. Refinements to various facets of thunderstorm structure are still underway. One such component still under investigation is that of thunderstorm outflow.

1.3 Outflow and Downdraft Structure

A distinction is often made between the terms "outflow" and "downdraft." For the purposes of this paper, it shall be assumed that "outflow" is the more general term, referring to all the air leaving the storm regardless of direction of flow. The term "downdraft" shall refer to that portion of the outflow associated with the main echo and having a marked downward component of motion.

The mechanisms which form and maintain the downdraft have been the subject of considerable speculation and research. Near the

---

*The term "weak echo region" had, by this time, been substituted for the term "echo free vault," since the region in question did contain small cloud droplets (and thus could produce an echo) even though the region would appear "echo-free" to a radar equipped only to detect larger precipitation particles.

beginning of the 20th Century, Humphreys (1914) suggested that downdrafts formed as a result of cold rain and hail falling from near cloud top through the warmer cloud air below. The downdraft was thus postulated to occur via three mechanisms, namely: (1) frictional drag induced by the falling drops, (2) an increase in air density resulting from conductive cooling of the column by the cold particles and (3) a further increase in density due to evaporation of the descending drops.

As previously mentioned, Byers and Braham (1948) studied several storms in Florida and Ohio. Their conclusions agreed generally with those of Humphreys, indicating that he was essentially correct in his analysis. Byers and Braham found, however, that an essentially ignored process (i.e., entrainment) also played an important role in the downdraft. Furthermore, they also noted that while an updraft might extend all the way to cloud top, downdrafts originate below ~25,000 feet.

As discussed in the preceding section, Ludlam (1963) presented a "state of the art" synopsis of the thunderstorm. Ludlam's contention that vertical wind shear is a significant factor for the occurrence of severe local storms forms an important part of the downdraft arguments herein.

Contrary to previous speculation that the strong downdrafts formed chiefly from cloudy air modified by precipitation, Newton (1966) argued that, in fact, entrainment was the primary factor. Newton began his argument by demonstrating that the updraft core in severe thunderstorms

must remain fundamentally undiluted from cloud base to near cloud top. He based this contention on the fact that the height reached by the updraft (in a case study of a severe squall line thunderstorm) agreed very well with the height predicted by undiluted parcel theory. Then, utilizing thermodynamic arguments, he showed that it would be nearly impossible for this undiluted updraft air reaching cloud top to return to the lower troposphere via any known mechanism. Consequently, the downdraft must have its primary source elsewhere. (He did conclude, however, that, due to vertical wind shear, the updraft leans in an upshear sense, making it possible for some condensed water to fall from the updraft into the downdraft region.)

In searching for a source of the downdraft air, Newton compared the θ_w values found in the surface outflow to those of the environment. He discovered (as had earlier investigators) that θ_w values appearing in the surface outflow corresponded to θ_w values at mid-cloud level (i.e., 400-650 mb).

On this basis, Newton postulated a separate circulation for the downdraft--its main source being horizontally entraining mid-level air which becomes negatively buoyant upon entering the storm environment. The updraft (tilted in an upshear sense) deposits condensed water into this intruding stream of air and chills it even further through evaporation. The consequent gravitational sinking of the denser air possessing a large horizontal momentum becomes the mechanism for the formation of the micro-scale cold front which, in turn, undercuts and regenerates the updraft.

The dynamical model upon which the present analysis is based is that of Newton (1966) and is presented schematically in Figure 1.3.

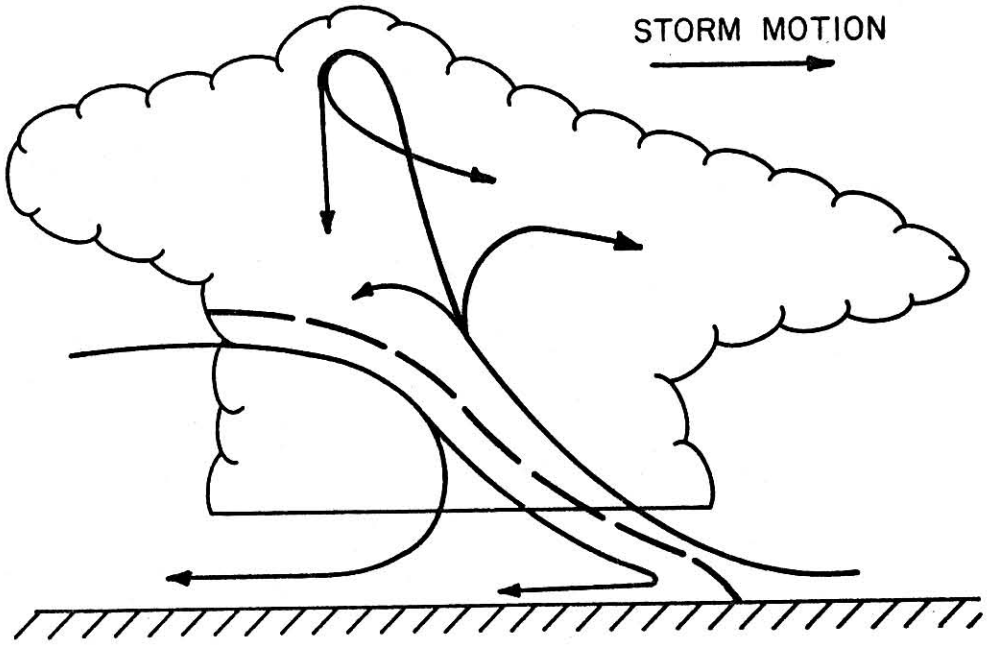

Figure 1.3 Vertical cross-section of a single storm in a squall line illustrating the principal branches of air circulation (after Newton, 1966).

CHAPTER II

OBSERVATIONAL SYSTEMS

2.1 Introduction

The case study of 22 July 1973, was conducted as part of the University of Wyoming's participation in the five year National Hail Research Experiment (NHRE) which was supported by the National Science Foundation (NSF). The general goals of the NHRE were to increase man's understanding of the dynamics and microphysics of severe local storms and to thereby develop a practical method of suppressing damaging hail. Field headquarters for the NHRE was located in northeastern Colorado near the town of Grover.

2.2 Data Collection

Synoptic data. National Weather Service (NWS) synoptic data were used in a supportive fashion for the case described in this paper. Because these data were not critical to the final conclusions, measurement errors were not critically evaluated.

Mesonetwork data. In addition to the NWS synoptic data, the NHRE operated a surface mesonetwork consisting of 33 stations in the area under consideration. These stations were located from Grover east in a grid pattern covering an area of $\sim$3000 km^2 (Figure 2.1). Pressure, temperature, relative humidity and winds were recorded at each site on 24-hour strip charts. Instrumentation at each site consisted of:

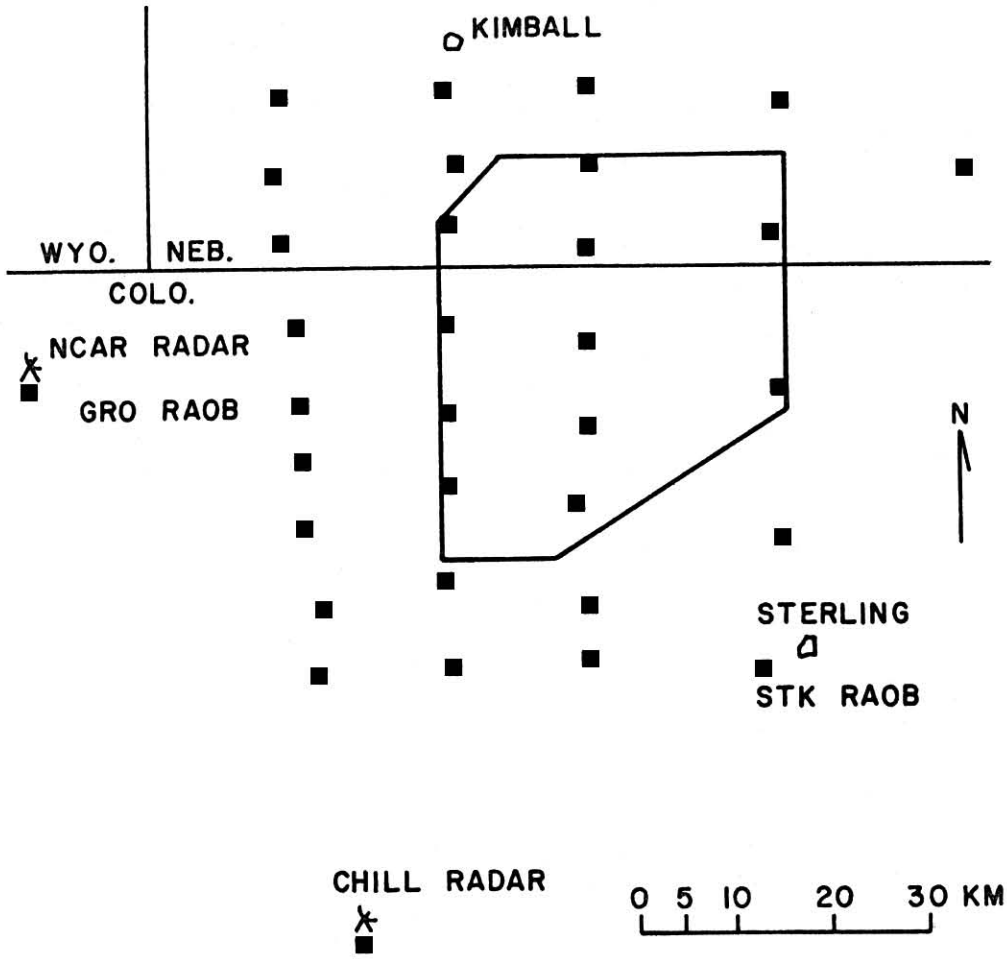

Figure 2.1 The NHRE surface mesonetwork and the Protected Area. Boxes indicate mesonet stations. NCAR and CHILL radar sites sites are also shown. Grover and Sterling, Colorado rawinsonde release sites are located at the mesonet stations indicated.

1. Climet Wind System, providing measurements of wind speed and direction with an error of ±2 km/hr (speed) and ±2° (direction).
2. Epic thermograph, measuring temperature to within ±0.5C*.
3. Serdex hygrograph, employing a diffusion membrane to record relative humidity with an error of ±4%*.
4. Belfort microbarograph, measuring pressure in millibars (±1 mb).

Mesonetwork instruments were extensively calibrated at the beginning and end of each operational year. Additionally, each functioning station was visited at least once a day to change the charts, as well as to calibrate the time, temperature, humidity and pressure. Necessary preventative maintenance was also performed during these visits.

Upper air data. Routine NWS rawinsonde data were available for the case presented in this paper. Data were also available from the NHRE radiosonde release sites near Grover (GRO) and Sterling (STK), Colorado. Both Grover and Sterling sites operated seven days a week with routine releases at 0800 MDT, 1100 MDT, 1400 MDT and 1700 MDT.

Radiosonde temperature values (unsaturated) were accurate to within ±0.5C (e.g., Lenhard, 1970). Relative humidity measurements were considered accurate to within 4% (as opposed to the normally assumed 5%) because of an improved air intake duct designed by Friedman (1972).

---

*T. R. Nicholas, staff member, NHRE, personal communication.

Radar. Two research radar systems for measuring reflectivity factors were operated concurrently during the 1973 NHRE season--the NCAR radar near Grover and the CHILL radar (University of CHicago-ILLinois State Water Survey) near Fort Morgan. Although both systems monitored storms at two wavelengths (3 cm and 10 cm), only the S-band (10 cm) wavelength data were used in the present analysis. Average log reflectivities were recorded digitally on magnetic tape for later computer processing.

Characteristics for the NHRE radar were as follows:

	NCAR	CHILL
Type of radar	CPR-2	AN/FPS-18 (mod.)
Peak transmitted power, kw	1000	600
Beamwidth, deg	0.85	0.85
Wavelength, cm	10.7	10.7
Pulse repetition frequency, PPS	1071, 1250	974
Operational scan modes	PPI	PPI

Both of the NHRE radar systems were found to contain certain intrinsic errors. It was discovered that absolute reflectivity values reported by the NCAR radar were somewhat suspect. Two separate calibrations (and subsequent investigations) indicated a depressed gain in the receiver part of the system of $\sim$8dB. However, absolute reflectivity values were not critical in the present analysis so that these errors did not affect the results.

Calibration tests performed on the CHILL radar system showed that its reflectivities were in error by a factor of ∿2dB. Furthermore, due to a faulty memory element in the CHILL processor, an azimuth distortion of the PPI presentation appeared in the computer output from the CHILL system. As in the case of the NCAR errors, neither the reflectivity error nor the azimuth distortion affected the results herein.

In addition to the aforementioned systems, radar data from the NWS WSR-57 weather radar at Limon, Colorado (LIC), were used for intercomparison checks of the Grover and Fort Morgan radars. Furthermore, neither Grover nor Fort Morgan radars were focused continuously on the portion of the storm under consideration here, since they were both pursuing their primary objective, i.e., monitoring storms which might potentially deposit hail on the protected area (see Figure 2.1). Consequently, coverage by these two radars was rather sporadic. LIC data were thus also useful in furnishing a continuous overview of the complete storm system.

Aircraft. Four instrumented aircraft flew beneath the base of the cloud containing the cloud-free vault on 22 July 1973. They were the University of Wyoming Queen Air (N10UW), two NCAR Queen Airs (N304D and N306D), and the NCAR de Havilland Buffalo (N326D).

The Wyoming Queen Air was an instrumented twin-engine Beechcraft airplane equipped to measure and record the parameters of state, vertical winds and the aircraft parameters (i.e., manifold pressure, rate of climb, indicated air speed, turbulence and aircraft position relative to the ground). Crew members utilized voice recorders to describe

significant events and cameras to photograph visual events, when appropriate. Crew members also had access to an event coding system by which meteorological events (such as "enter cloud base," "encounter precipitation," "enter updrafts," etc.) could be registered as a permanent record when a specific event button was pushed. Ten different buttons representing separate events were available for use by each crew member. The flight path of N10UW was reconstructed from the recorded DME and VOR. The VOR-DME positioning system was felt to be accurate to $\pm 1°$ (direction) and 0.2 km (distance). For a detailed discussion of the instrumentation on N10UW, refer to Endsley and Knowlton (1973). A listing of the aircraft's instrumentation is given in Appendix A.

With a few important variations, the parameters (and accuracies thereof) monitored by the NCAR Queen Airs were nearly identical to those gathered by N10UW. One exception was that neither N304D nor N306D were equipped to measure vertical winds. On the other hand, both of these aircraft recorded horizontal winds using a Doppler radar navigational system. The Doppler system also formed the basis for calculating and recording flight paths for the NCAR Queen Airs. To obtain aircraft positions with time, the output from the Doppler system is integrated. All errors, whether discretely or continuously created, are thus accumulated. Since the Doppler data are quite unreliable during turns, most of the positioning errors were accumulated. However, the NCAR Queen Airs flew paths which intermittently crossed the path of the Wyoming Queen Air several times between 1700 and 1725 MDT, and it was

possible to adjust the flight tracks during this period. Positioning accuracy for the corrected tracks is assumed to be $\sim\pm 1$ km. After 1725 MDT the NCAR Queen Airs flew in formation with the NCAR Buffalo (N326D). Therefore, positions for N304D and N306D could be inferred from flight track data of the Buffalo, whose position (as discussed below) was known to a high degree of accuracy. By this method any intrinsic errors in the NCAR Queen Airs' positioning systems were not important. A complete list of the instrumentation appears in Appendix A.

The NCAR Buffalo was equipped to monitor the parameters of state, both vertical and horizontal winds and the aircraft parameters. Position keeping was obtained with an Inertial Navigational System. The flight track reconstructed via this system was based on changes in aircraft position relative to position at take-off. These changes in position are computed from instrumentally derived, three-dimensional velocity vectors. The accuracy of points thus calculated are assumed to be $\sim$1.5 km hr^{-1} of flight due to the high accuracy of the computed velocity vectors. A listing of this aircraft's instrumentation can be found in Appendix A.

It should also be noted that none of the NCAR aircraft had event coding systems or voice recorders to aid in the later interpretation of ambiguous data.

Since instrumentation on the four aircraft differed somewhat, it was necessary to perform inter-comparison tests to establish that the four aircraft were recording identical values for the parameters under

consideration. Two different procedures were employed toward this end.

The first test consisted of aircraft flights past a well calibrated, instrumented tower (located six miles south of Grover) to compare temperature, pressure and relative humidity. The second test consisted of a series of formal inter-aircraft comparison flights with all four planes flying in close formation. The reference aircraft for the inter-comparison of meteorological and aircraft variables was the NCAR Buffalo. No other tests were required to establish the interchangeability of these data (Biter and Wade, 1975).

CHAPTER III

CASE STUDY - 22 JULY 1973

3.1 Introduction

A severe squall line occurred on the afternoon of 22 July 1973 in the vicinity of the NHRE storm monitoring network, headquartered near Grover, Colorado. Several isolated storms also formed near the southernmost end of this squall line.

Meteorological conditions which prevailed early in the day indicated that strong storm potential existed. The morning (0600 MDT) 500 mb analysis showed a long wave trough positioned over the western United States. A relatively weak short wave (with an associated surface cold front) was superimposed on this major disturbance and was approaching the NHRE study area from the west. Resultant wind flow above 600 mb was generally southwesterly over the area (Figure 3.1). Proximity rawinsonde data (Figure 3.2) indicated that strong conditional instability was present in the atmosphere, but was capped by a stable layer near cloud base. The temperature and pressure at cloud base were 12C and ∿760 mb, respectively, as determined by instrumentation onboard the Wyoming Queen Air. This corresponds to an equivalent potential temperature value of 343.5 K.

The squall line which developed slightly ahead of the rapidly moving surface cold front formed in a rather peculiar manner. The northern segment of the squall line formed with an orientation nearly

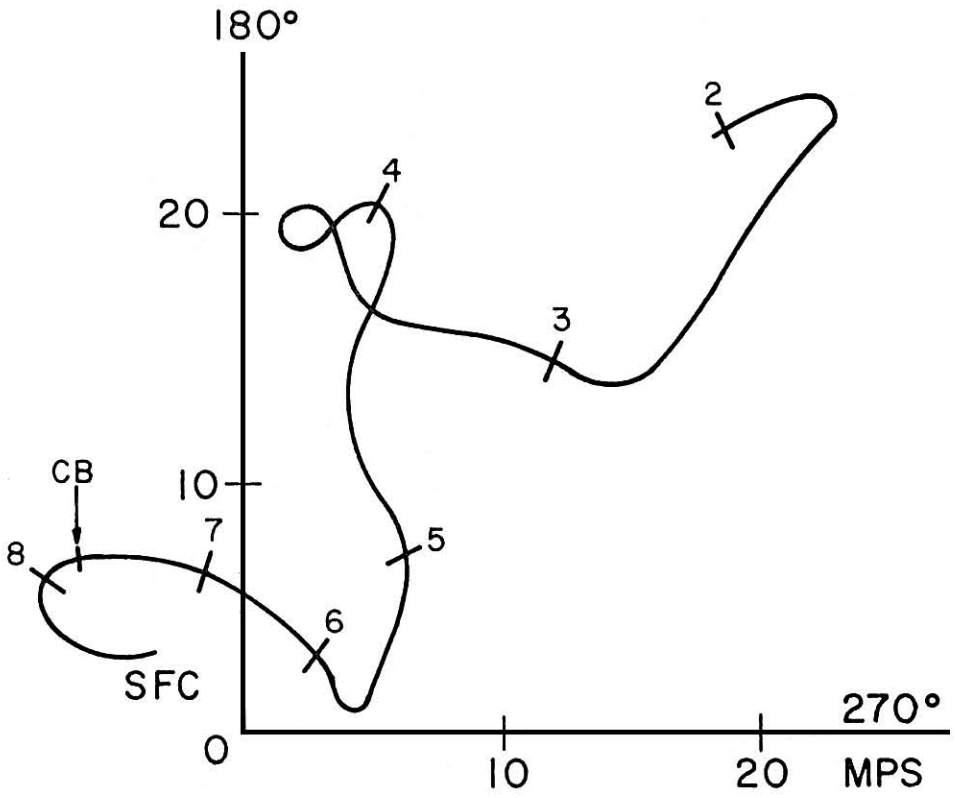

Figure 3.1 Hodograph from the 1630 MDT Sterling, Colorado rawinsonde release. Indicated are levels of 100 mb increments. CB refers to cloud base.

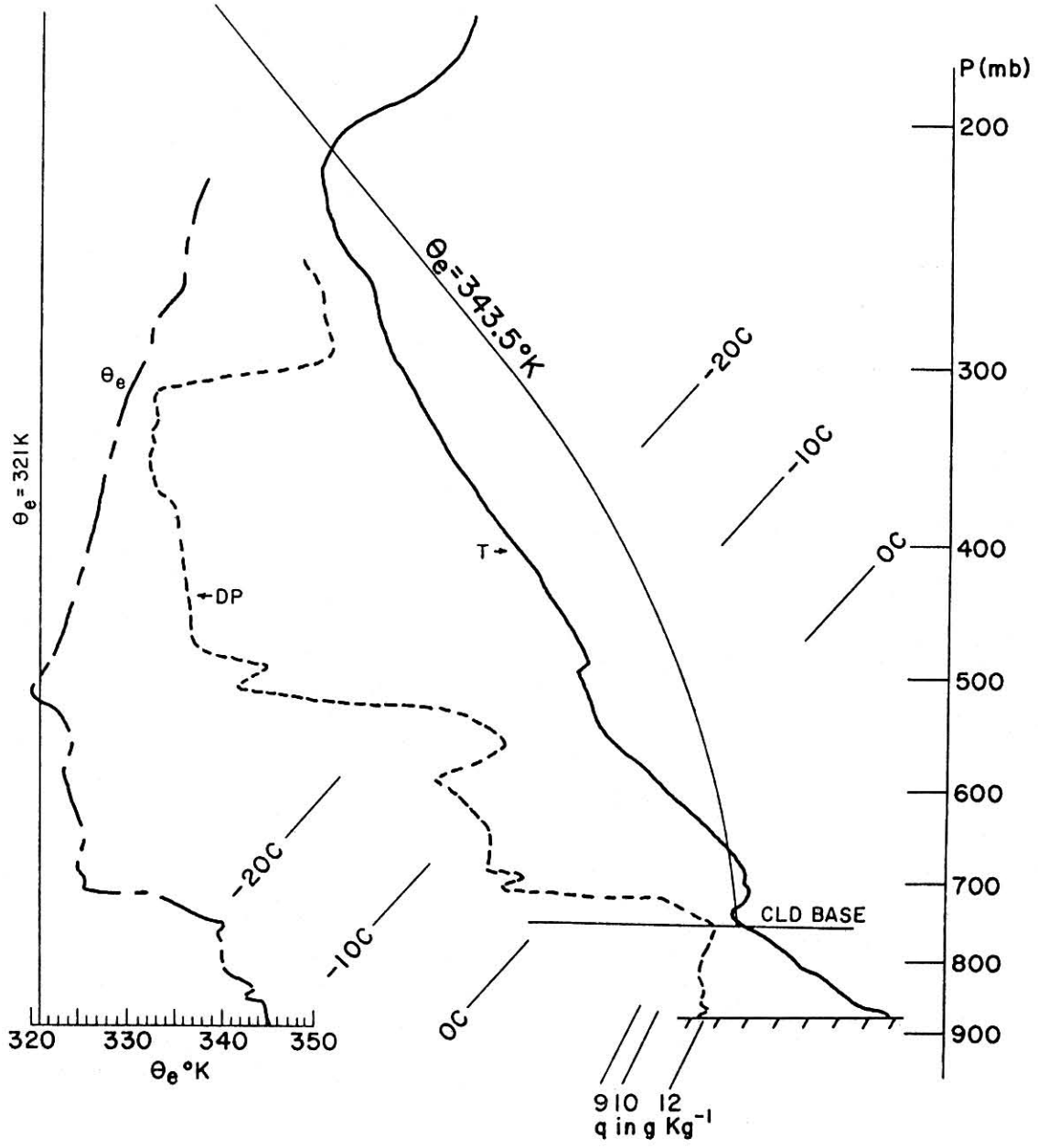

Figure 3.2 Sterling, Colorado sounding at 1630 MDT plotted on a Skew T-Log p diagram. Temperature (T) and dew point (DP) traces as indicated. Also shown is the vertical profile of θ_e. θ_e at cloud base was 343.5 K.

parallel to the cloud level winds (i.e., NE-SW), while the southern segment was aligned N-S (Figure 3.3). A group of isolated storms was located southeast of this line.

Several small tornadoes and funnel clouds, large hail (e.g., as reported near Cheyenne, Wyoming at 1700 MDT by the CYS reporting station) and a strong gust front occurred in association with the southern segment of the squall line. The isolated storms also developed strong gust fronts. These gust fronts will be discussed later. However, according to both voice tape notes from N10UW and aircraft data from all four aircraft, the northern segment did not form a gust front. Instead, it acquired a large visual cloud free vault between the precipitation curtain and the shelf-like updraft pedestal (Figures 3.4 and 3.5).

This vault on the Grover squall line expanded to a width of ∿10 km, a length of ∿60 km and extended vertically some 0.6 km above the base of the updraft pedestal, i.e., the lifting condensation level. The length was estimated by observers onboard N10UW; width and height were determined from aircraft data obtained during vault penetrations. In addition to the well defined updraft pedestal (see Figure 3.5c), a most distinctive visual feature was the vault's "roof." As may be seen in the photographs (Figure 3.5), the clouds composing the roof displayed a very ragged, scalloped appearance. These formations might easily be mistaken for mammatus, but when observed at close range from aircraft they do not exhibit mammatus characteristics. An extensive diffusion of sunlight shining through the roof indicated that the cloud layer capping the vault was very thin.

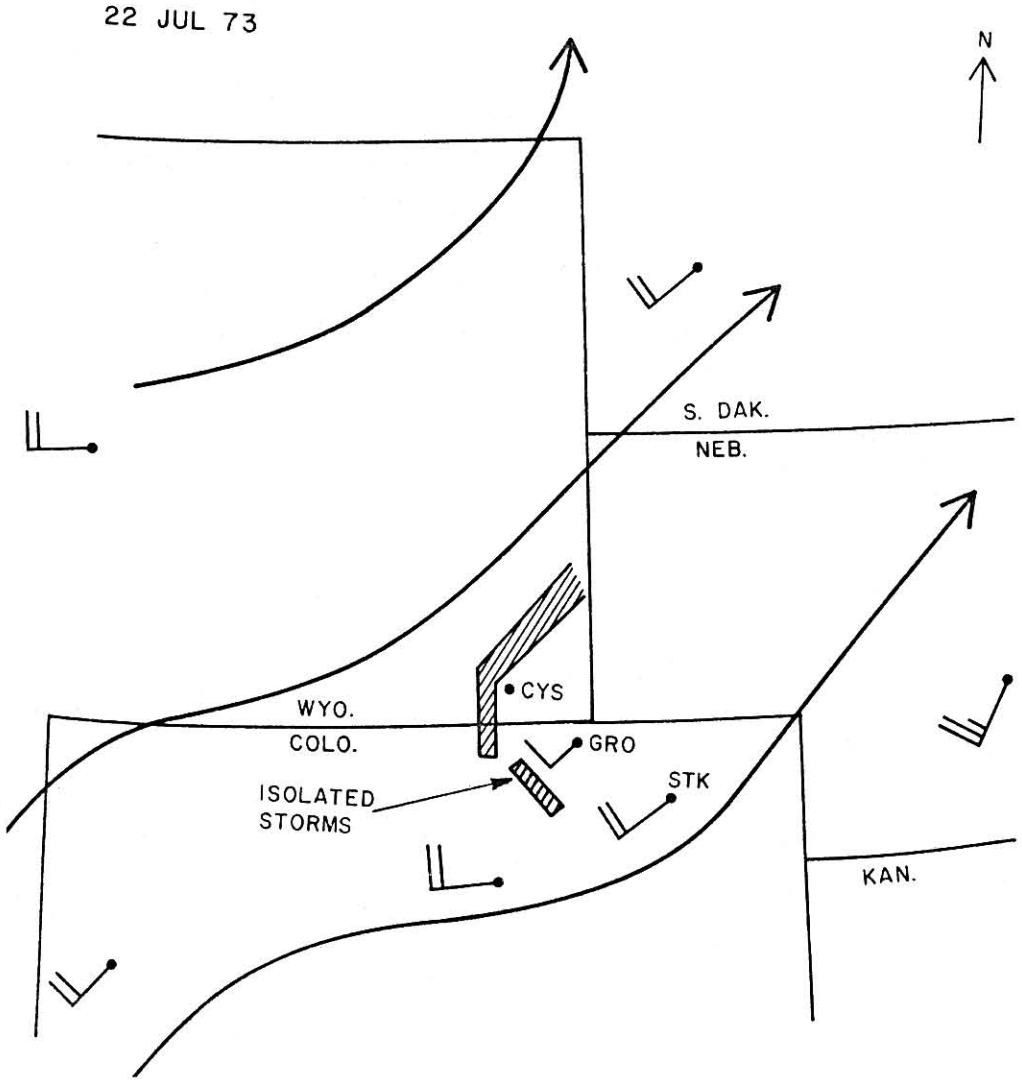

Figure 3.3 Colorado and surrounding states showing the 500 mb wind barbs and streamlines from the 0600 MDT NWS summary. Superimposed are wind data from Grover and Sterling, Colorado 1630 MDT radiosonde releases. The squall line and the area of isolated storms are depicted schematically.

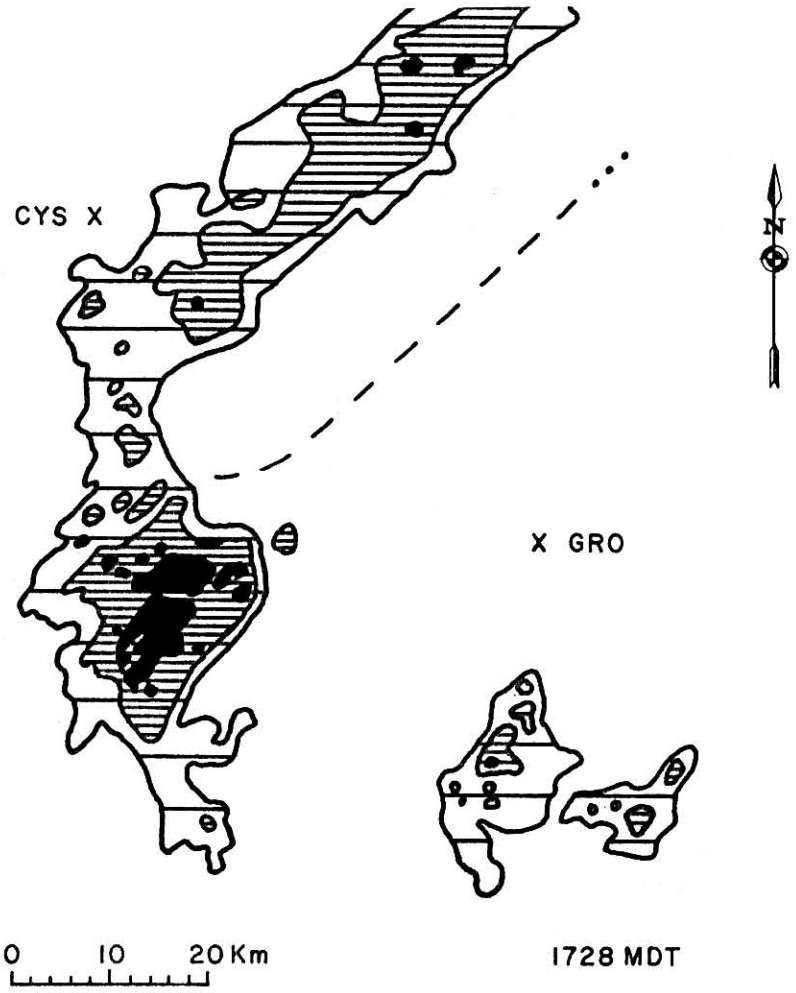

Figure 3.4 Cloud base PPI radar presentation taken from the CHILL radar at 1728 MDT. Contour intervals are 10dBz beginning at 20 dBz. Dashed line represents the leading edge of the cloud free vault.

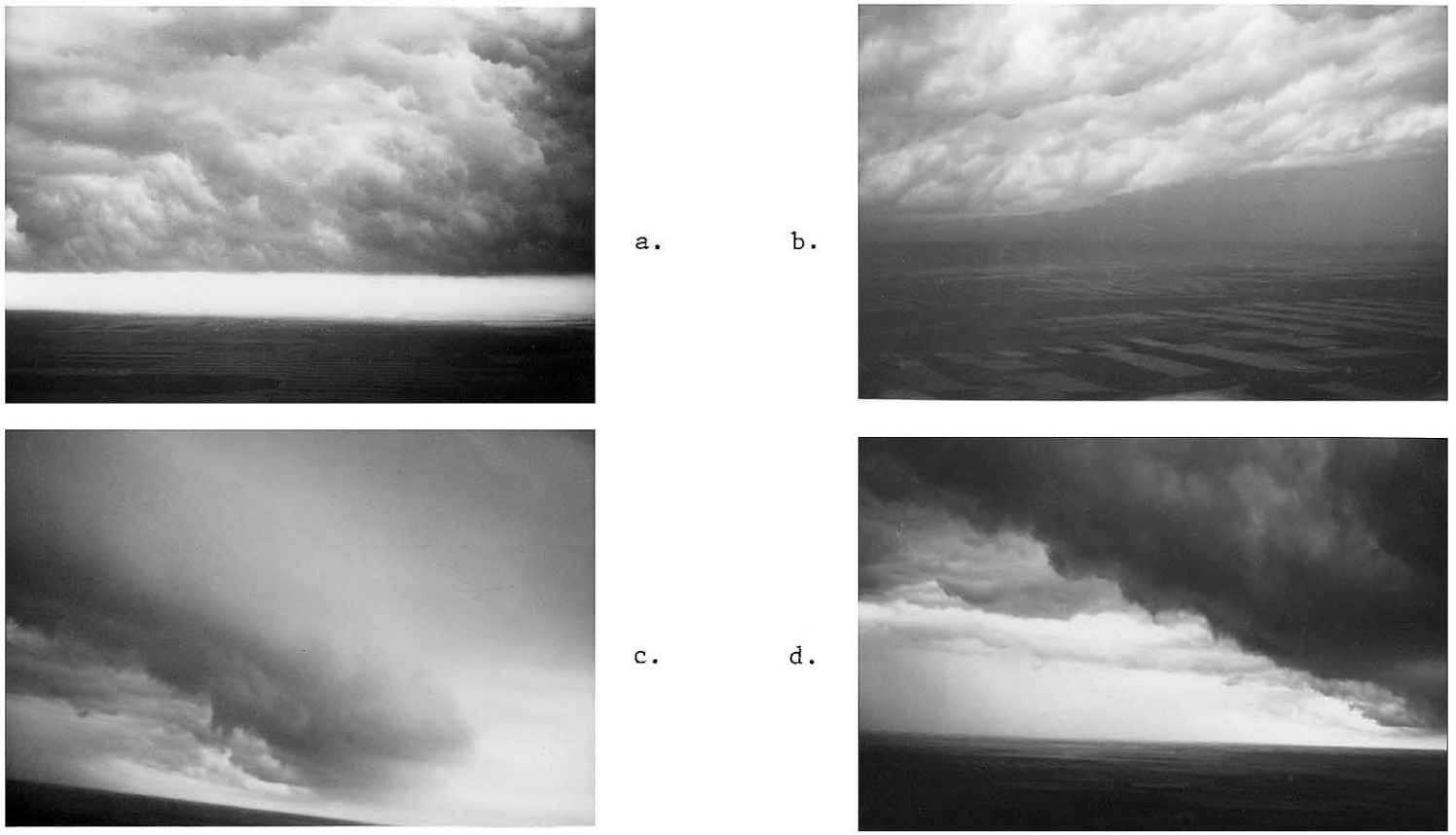

Figure 3.5 Photographs of the cloud free vault at (a) 1734 MDT looking east-southeast from inside the vault (see Figure 3.6), (b) 1810 MDT looking southeast along front edge of vault (Figure 3.7), (c) 1744 MDT looking north toward the shelf-like updraft pedestal along the leading edge of the vault (Figure 3.6) and (d) 1745 MDT along the leading edge of the vault showing the slope of cloud base near the vault (Figure 3.6).

3.2 Data Synthesis

Thermodynamic and kinematic data from three regions--the inflow air, the air within the cloud free vault and the gust front air near the southern segment of the squall line were synthesized.

The cloud free vault. Two separate penetrations of the cloud free vault were made by the Wyoming Queen Air--one constant altitude pass at ∿2.3 km MSL (Figure 3.6) and another flight spiraling upward from near ground level to an altitude of ∿2.7 km MSL (i.e., 0.2 km below the roof of the vault) as shown in Figure 3.7. Data collected during these two flight segments are shown in Figures 3.8 and 3.9.

At the time of the first vault penetration (∿1730 MDT) by N10UW, the NCAR planes were flying just ahead of the leading edge of the vault. Examination of horizontal wind (as well as thermodynamic) data obtained during this period by the NCAR planes showed that the region near the cloud pedestal was an inflow zone. These data, in conjunction with data gathered by N10UW as it passed beneath the pedestal, furnished justification for referring to this structure as an "updraft" pedestal.

During the eight minutes preceding the second vault penetration (∿1806 MDT), N10UW descended through the environment immediately ahead of the storm from an altitude of ∿3.6 km MSL to near ground level. This descent furnished sounding data for the air directly ahead of the advancing storm. By combining these sounding data with those from within the vault, and assuming the vault to be approximately steady-state for this twenty minute period, it was possible to synthesize a complete vertical profile of the phenomenon.

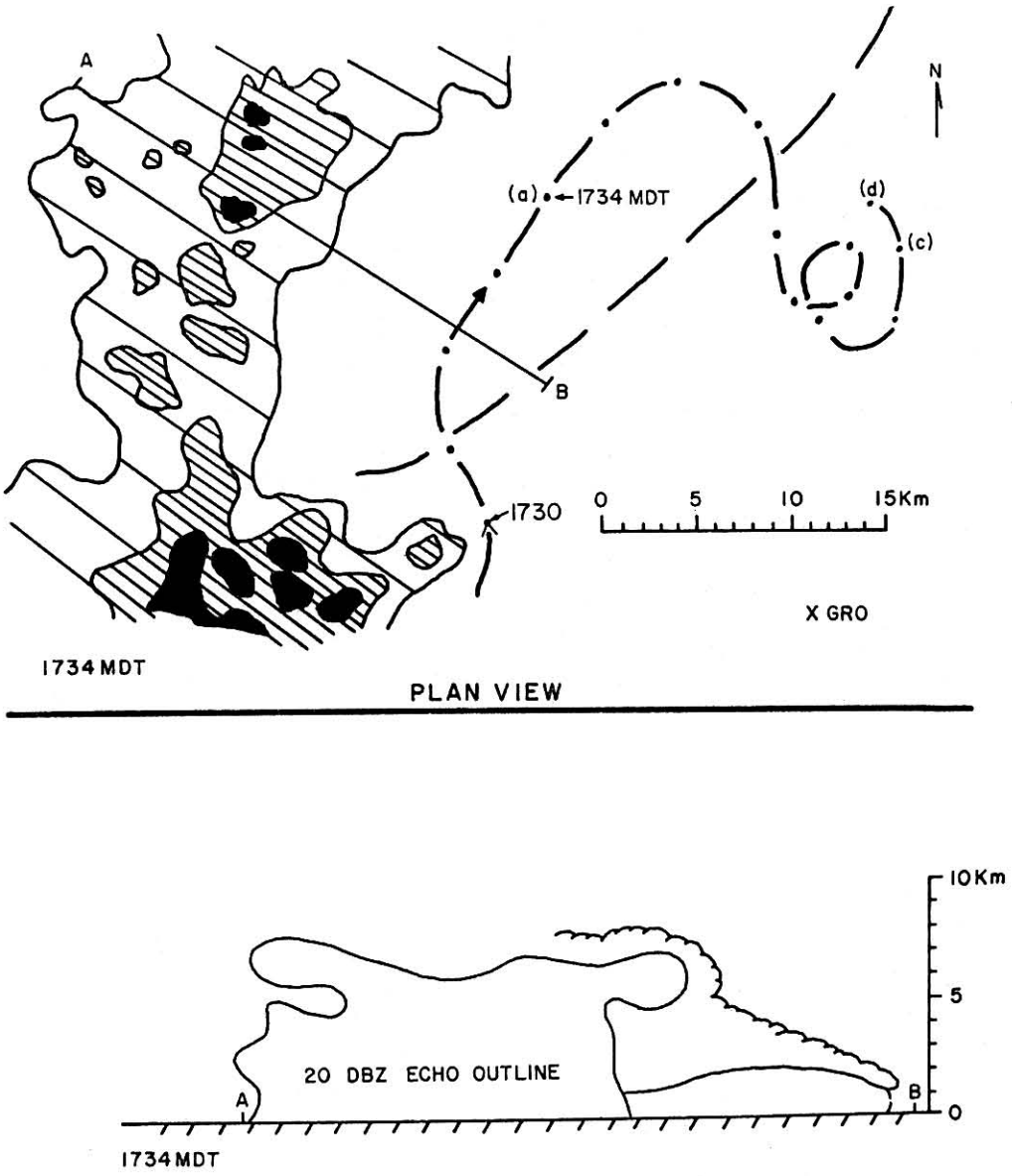

Figure 3.6 Plan view and vertical profile of the storm at 1734 MDT. PPI radar echo from the CHILL radar. Dashed line represents the leading edge of the cloud free vault. Dot-dash line depicts the flight path of the Wyoming aircraft from 1729 to 1745 MDT relative to the storm. Dots are placed at one minute intervals. Small letters (a), (c) and (d) represent the position of the plane at the time the corresponding photographs in Figure 3.5 were taken. The vertical profile is a composite of horizontal scans from 1734 to 1736 MDT along line A-B as indicated in the plan view.

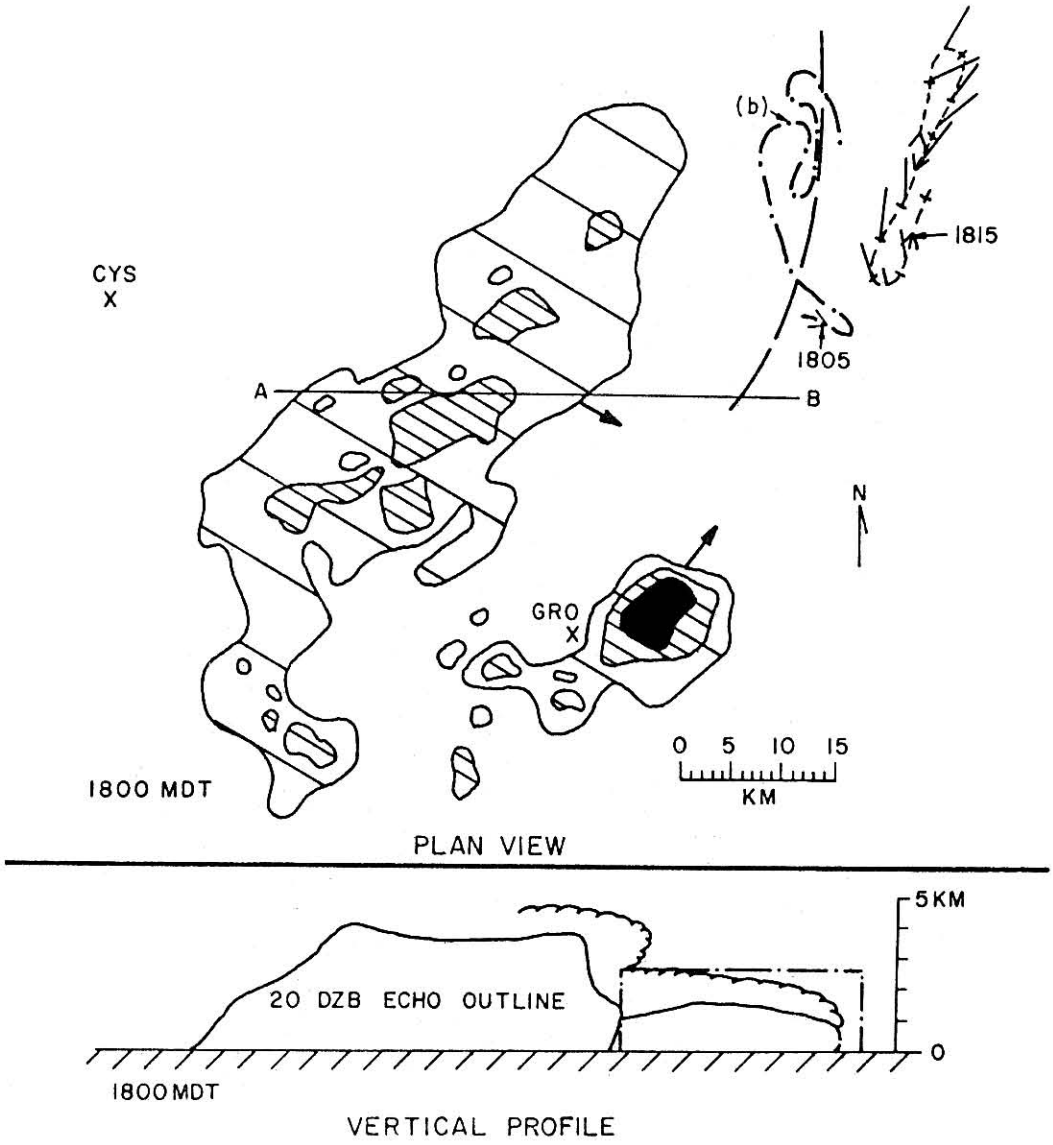

Figure 3.7 Plan view and vertical profile of the storm at ∿1800 MDT. PPI radar echo from the CHILL radar. Dashed line represents the leading edge of the cloud free vault. Dot-dash line depicts the flight path of the Wyoming aircraft from 1804 to 1817 MDT relative to the storm. Dots are placed at one minute intervals. Dotted line in upper figure represents the flight path of N326D, showing winds encountered at ∿0.8 km AGL. Direction represents wind direction. Length is proportional to speed (1 km = 2 m sec^{-1}). Small (b) shows the position of the plane at the time the corresponding photo in Figure 3.5 was taken. The vertical profile is a composite of horizontal scans along line A-B as indicated in the plan view. Vertical profile is exaggerated 2:1 in the vertical.

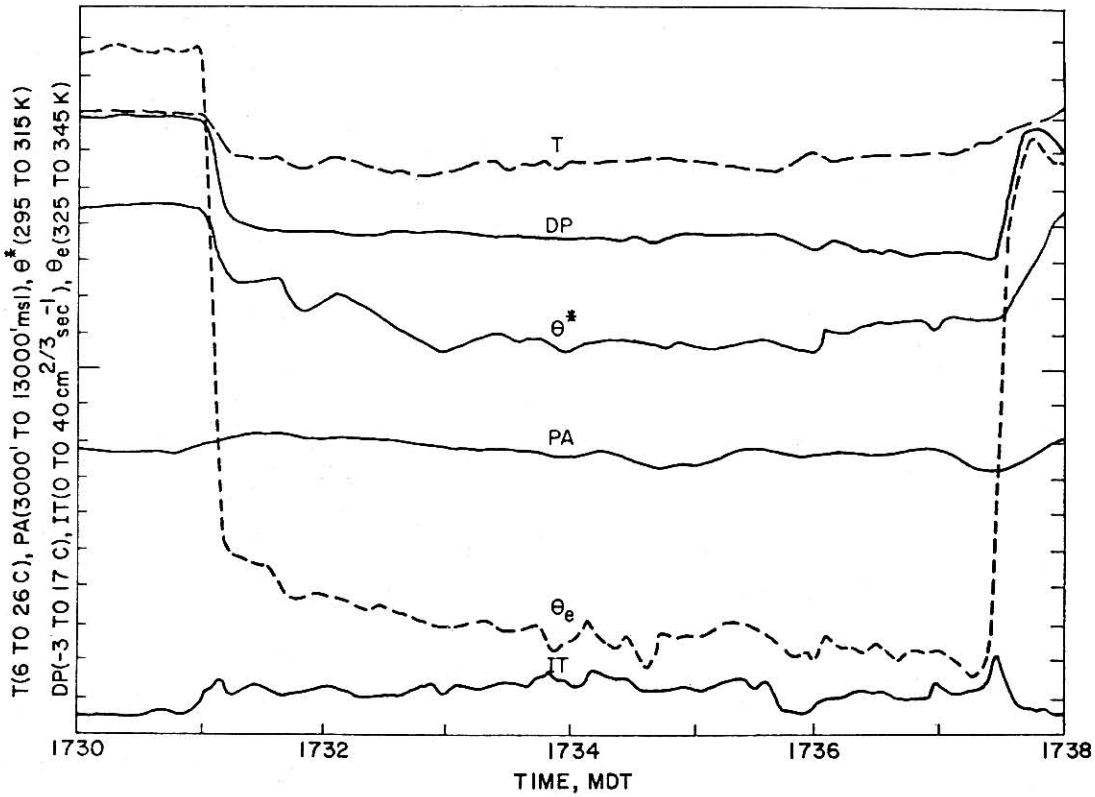

Figure 3.8 Time section from 1730 to 1738 of aircraft data (N10UW) for the vault penetration shown in Figure 3.6. Traces of temperature (T), dew point (DP), pressure altitude (PA), indicated turbulence ($IT = \varepsilon 0.33 \rho \rho_o^{-1}$), virtual potential temperature (θ^*), equivalent potential temperature (θ_e). ρ is the air density at flight altitude, ρ_o the air density at sea level and ε is the eddy dissipation rate of turbulent energy.

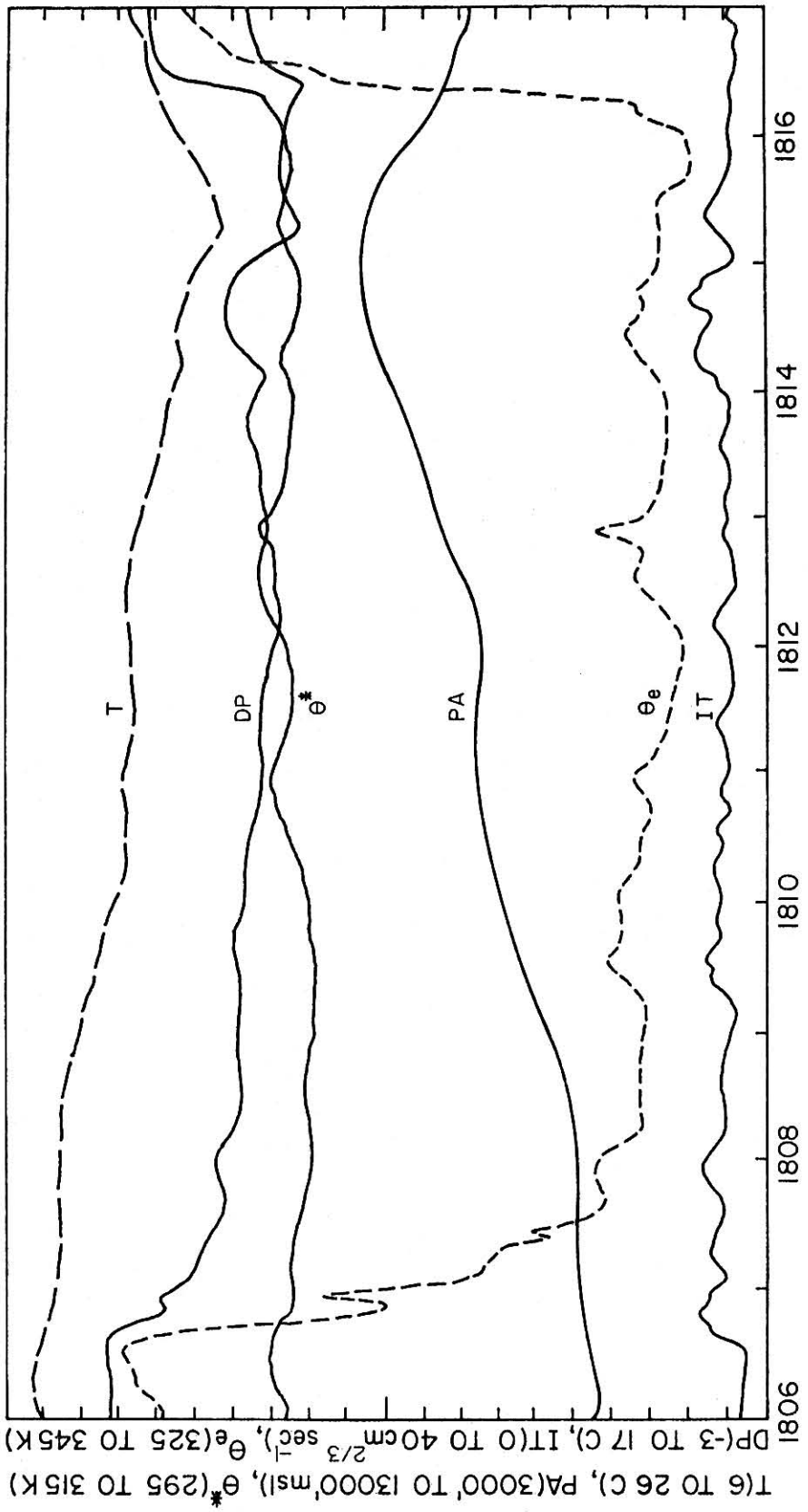

Figure 3.9 Time section from 1804 to 1817 of aircraft data (N10UW) for the vault penetration shown in Figure 3.7. Otherwise, same as Figure 3.8.

During this time period the NCAR aircraft were attempting to fly slightly ahead of the vault, but were inadvertently passing in and out of vault air. Data collected during this time showed winds to be light and variable along this boundary (Figure 3.7).

Data collected from both vault passes clearly indicated a well defined boundary between the inflow air and the air within the vault. The shape of this boundary (or "nose") is assumed to be similar to the model developed by Charba (1974) for outflow air. In the vertical cross-section (Figure 3.10), this boundary is defined by strong horizontal gradients of specific humidity (q), potential temperature (θ), equivalent potential temperature (θ_e) and virtual potential temperature (θ^*). The data also showed that the air within the vault contained no significant updrafts or downdrafts and was generally quiescent and non-turbulent, both as described verbally by aircraft crew members and as measured by the N10UW UITS system. Recorded Indicated Turbulence was $IT \leq 2\ cm^{2/3}\ sec^{-1}$, which corresponds to light turbulence (MacCready, 1964, as adapted to N10UW by Marwitz, 1972).

Examination of these results (Figure 3.10) leads one to speculate on the source of the air in the cloud free vault. Of the several possible explanations, most can be logically eliminated. First, the vault air could not have entered directly from the environment ahead of the storm because of differences in the derived state parameters across the boundary of the nose. Neither could the air have descended through the roof of the vault. Were this the case, the vault roof would have evaporated. With these two possibilities discarded it becomes obvious that

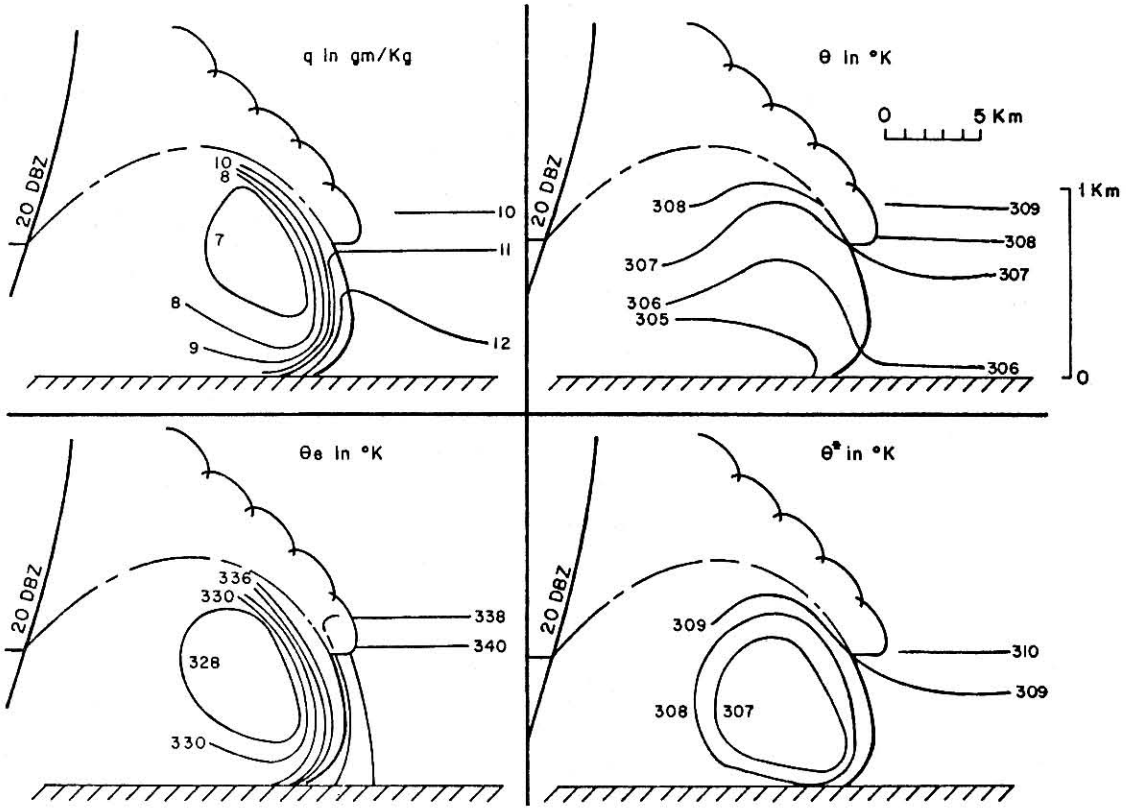

Figure 3.10 Vertical cross section (scaled 10:1) of the cloud free vault at ∿1800 MDT. The region shown is that outlined by the dotted rectangle in Figure 3.7. The leading edge (with respect to storm motion) of the 20 dBz echo is shown as well as the visual cloud free vault. The heavy black line on the nose of the vault represents the boundary between the vault air and the inflow. Thin black lines in each of the four parts illustrate the fields of specific humidity (q), potential temperature (θ), equivalent potential temperature (θ_e) and virtual potential temperature (θ*).

the air in the cloud free vault must have come from the downdrafts of the storm. However, the origin of this downdraft is still in question.

As to whether the vault air could have resulted strictly from a pseudo-adiabatic process, one must first consider the conservative nature of θ_e. It is known (e.g., Hess, 1966) that θ_e is a conservative property for atmospheric processes in which external heat or moisture is neither added to nor taken away from the parcel of air under consideration. Thus, had the vault air entered the storm as inflow, undergone a pseudo-adiabatic precipitation process and exited as outflow into the vault, one would expect to find θ_e values on either side of the boundary of the nose to be equal. As may be seen in Figure 3.10, there is a difference in θ_e of 12C across this boundary. It is, therefore, concluded that the air within the vault might have had its primary source in the inflow, but must have undergone at least some modification through a non-adiabatic mechanism.

Two non-adiabatic processes (which might affect the inflow air on its way through the storm toward the cloud free vault) were considered. They were conductive cooling of low and mid-level storm air by cold precipitation from above and the entrainment of air from outside the storm.

A close look at the process of conductive cooling was deemed necessary. Calculations were made based on a form of the equation for thermal conduction (e.g., Byers, 1965). The heat lost to the air, Q, by a drop of water at a different temperature is given by

$$Q = 4\pi r_d \lambda \gamma \Delta T \qquad (3.1)$$

where r_d is the radius of the drop, ΔT is the difference in temperature

between the drop and the air, λ is a constant depending on the nature of the substance (designated the thermal conductivity) and γ is a ventilation factor inserted to account for the effect of forced convection.

In order to estimate the heat transferred by conduction, raindrops with radii of 1 mm were assumed to occur in a concentration of 3 drops per liter. This represents a liquid water content of $\sim$12 gm kg^{-1}, which is felt to be an exaggerated value for the storm under consideration (e.g., see the specific humidity analysis in Figure 3.10).

ΔT was estimated in the following manner. The heat stored by a 1 mm radius drop of water can be shown to be,

$$H = 4/3\ \pi r_d^3 \rho_L c_L T \tag{3.2}$$

where ρ_L is the density of water and c_L the specific heat of water. The time derivative of (3.2) is simply the heat flux and is therefore equal to (3.1) or,

$$\frac{d}{dt}\left(\frac{4}{3}\ \pi r_d^3 \rho_L c_L T\right) = -4\pi r_d \lambda \gamma \Delta T$$

$$\text{or, } \frac{dT}{dt} = -\frac{3\lambda\gamma\Delta T}{\rho_L r_d^2 c_L} \tag{3.3}$$

$$\text{but, } \frac{dT}{dt} \equiv \frac{dT}{dz} \cdot \frac{dz}{dt} \tag{3.4}$$

Solving (3.3) and (3.4) simultaneously yields,

$$\Delta T = -\left(\frac{dT}{dz}\right)\left(\frac{dz}{dt}\right)\left(\frac{\rho_L r_d^2 c_L}{3\lambda\gamma}\right) \tag{3.5}$$

Assuming a drop of radius 1 mm (as previously stated), a lapse rate of 5.5C km^{-1}, a terminal vertical fall speed of 650 cm sec^{-1} (Mason, 1971)

and a ventilation factor of 8.5 (e.g., Ranz and Marshall, 1952) and using values for ρ_L of 1 gm cm^{-3}, c_L of $4.186(10)^7$ ergs gm^{-1} $°K^{-1}$ and λ of $(2.4)(10)^3$ erg cm^{-1} sec^{-1} $°K^{-1}$ yields upon substitution into (3.5) $\Delta T = -0.25C$ for this case.

Substitution of the above values into (3.1) produces (for a single drop),

$$Q = 4\pi r_d \lambda \gamma \Delta \simeq 6.4(10)^3 \text{ erg sec}^{-1}$$

With the previously assumed drop concentration of 3 drops per 10^3 cm^3, the total heat flux is,

$$Q_T = 19.2 \text{ erg sec}^{-1} \text{ cm}^{-3} \simeq 1.9(10)^4 \text{ erg sec}^{-1} \text{ gm}^{-1}$$

The specific heat capacity for moist air is,

$$c_p = 0.24(1 + 0.9q) \text{ cal gm}^{-1} °K^{-1}$$

$$(\simeq (10)^7 \text{ erg gm}^{-1} K^{-1} \text{ here})$$

By combining the total heat flux with the specific heat of air, it is found that the total cooling by conduction is $1.9(10)^{-3}$ per second.

As previously speculated, the air within the cloud free vault was outflow from the storm. However, due to the slow growth rate of the vault, it appears that the outflow must have been leaving the storm in a rather sluggish manner. Therefore, the "in storm" residence time of an air parcel entering the cloud as inflow and exiting into the cloud free vault might be as great as 30 minutes (an extreme value). With a residence time of 30 minutes, the conductive cooling could, at best, result in a loss of temperature by an air parcel of ≈3.4C. Thus, even with all variables exaggerated, conductive cooling could only account for 3.4C of the 12C difference observed. Calculations in

which hail particles were substituted for raindrops, yielded similar results. These estimations effectively eliminate conduction as a source for the major modification of θ_e.

By the preceding process of elimination, one is left with the only other choice--that of entrainment--as the major non-adiabatic mechanism by which the inflow could be modified. It is evident that the vault air (which contained θ_e values some 12C cooler and θ^* values $\sim$2C cooler than the inflow) was primarily a mixture of inflow air with entraining air.

The southern storm components. In contrast to the results obtained for the northern segment of the squall line, synthesis of mesonetwork and aircraft data from these southern components revealed large contrasts between the subcloud air ahead of the storms and the air behind the gust fronts. In Figures 3.11 and 3.12 are presented the results of analysis of surface mesonetwork data. Cold front positions and the spacing of gradients were obtained by space-time conversion of strip chart data. The analysis reveals two cold fronts. The E-W oriented front (Figures 3.11 and 3.12) crossed the mesonetwork first, moving from south to north. Gradients of thermodynamic properties behind this front were generally weak. Comparison of surface cold front data with radar data from the CHILL radar showed this air mass to be a remnant gust front from a storm which had dissipated at $\sim$1730 MDT. Subsequently, the second gust front (N-S oriented) entered the mesonet at $\sim$1820 MDT from the west and was associated with a strong cell (40-50 dbZ) located near Grover.

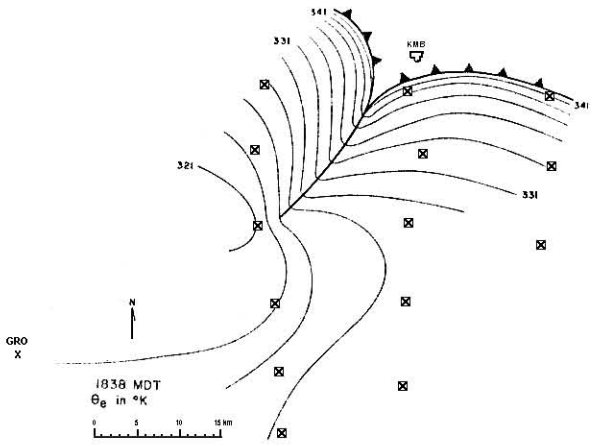

Figure 3.11 Surface analysis of θ_e at 1838 MDT based on time to space conversion of data from 14 NHRE mesonetwork stations.

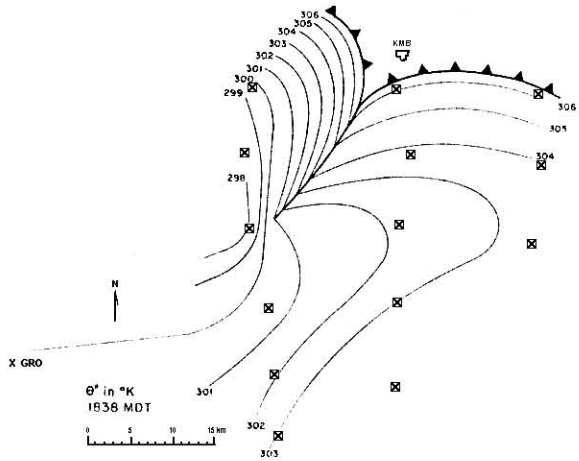

Figure 3.12 Analysis of θ* at 1838 MDT at the surface based on time to space conversion of data from 14 NHRE mesonetwork stations.

Surface analysis of θ_e at 1838 MDT (Figure 3.11) revealed a core of very low θ_e values (θ_e = 321 K) associated with the N-S oriented gust front. A lack of radar data from 1800 to 1855 MDT made it impossible to attribute this core of low θ_e air to a particular storm cell. However, comparison of both 1800 and 1855 MDT radar data with data gathered during this period by the NCAR aircraft made interpolation of storm position possible. Results from this interpolation showed that the core of low θ_e air had its origin from the southern components of the storm system, i.e., components which were more exposed to mid-level winds.

These low θ_e values were also observed by the NCAR aircraft. At ∿1825 MDT both N10UW and the NCAR aircraft terminated the storm study and started toward their respective home fields. Approximately seven minutes later (1832 MDT) and directly above the surface gust front, the NCAR fleet inadvertently encountered a region of extremely strong winds (Figure 3.13). (Compare to light and variable horizontal winds encountered near the cloud free vault--see Figure 3.7.) Synthesis of meteorological data collected during this encounter (Figure 3.14) disclosed that the values of θ_e encountered in the outflow at ∿0.8 km AGL were similar to those at the surface at the same time and location. Comparison of surface and aircraft sensed θ_e values obtained in the outflow with those of the environmental sounding (see Figure 3.2), shows that the gust fronts associated with the southern components of this system contained θ_e values corresponding to air in a shallow layer near 500 mb. Discounting the small amount of conductive cooling which might

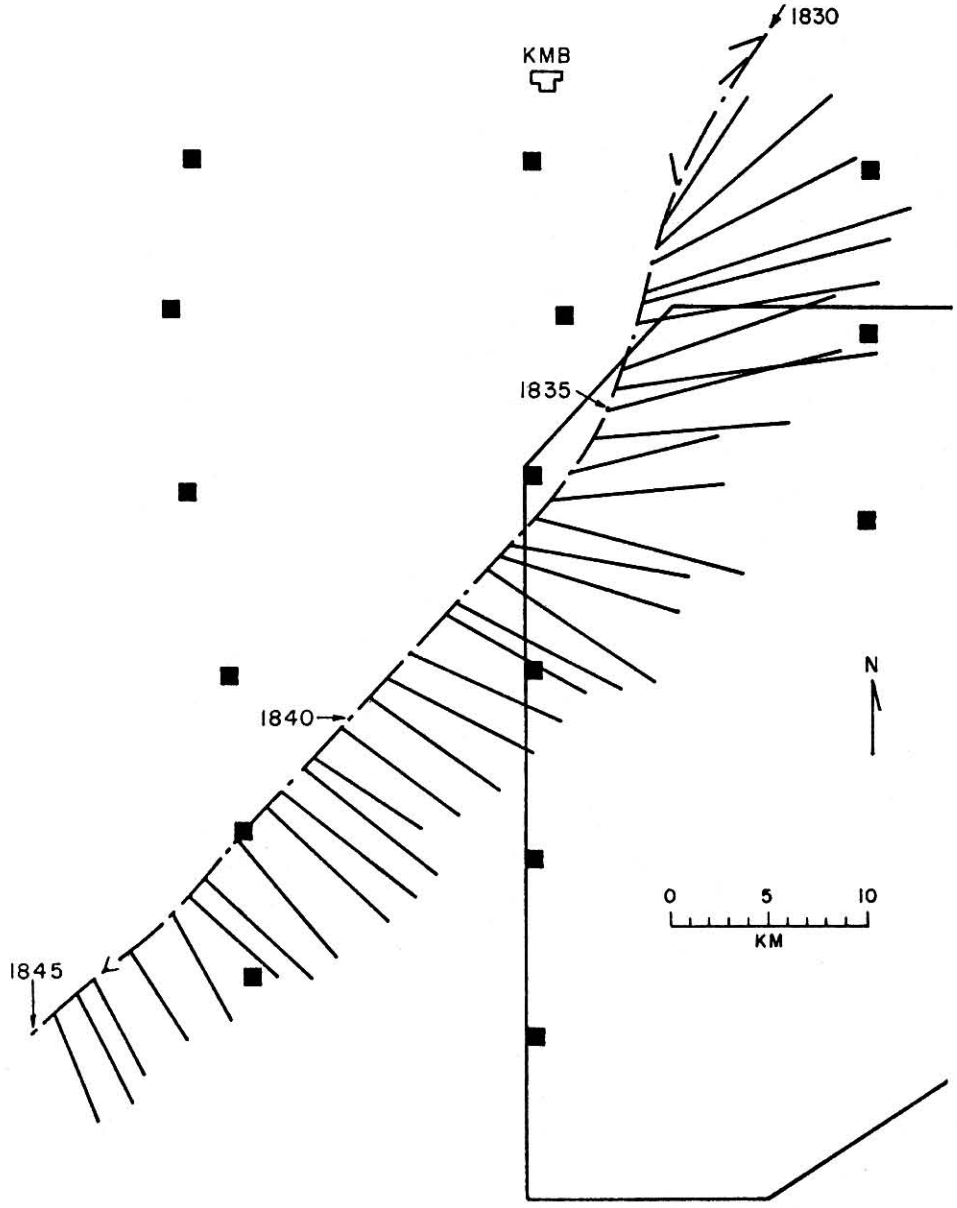

Figure 3.13 Flight path of N326D from 1830 to 1845 MDT showing gust front winds encountered at 1832 at 0.8 km AGL. Direction of wind barb represents wind direction. Length is proportional to speed (1 km = 2 m sec^{-1}). Dots on flight track are at one minute intervals.

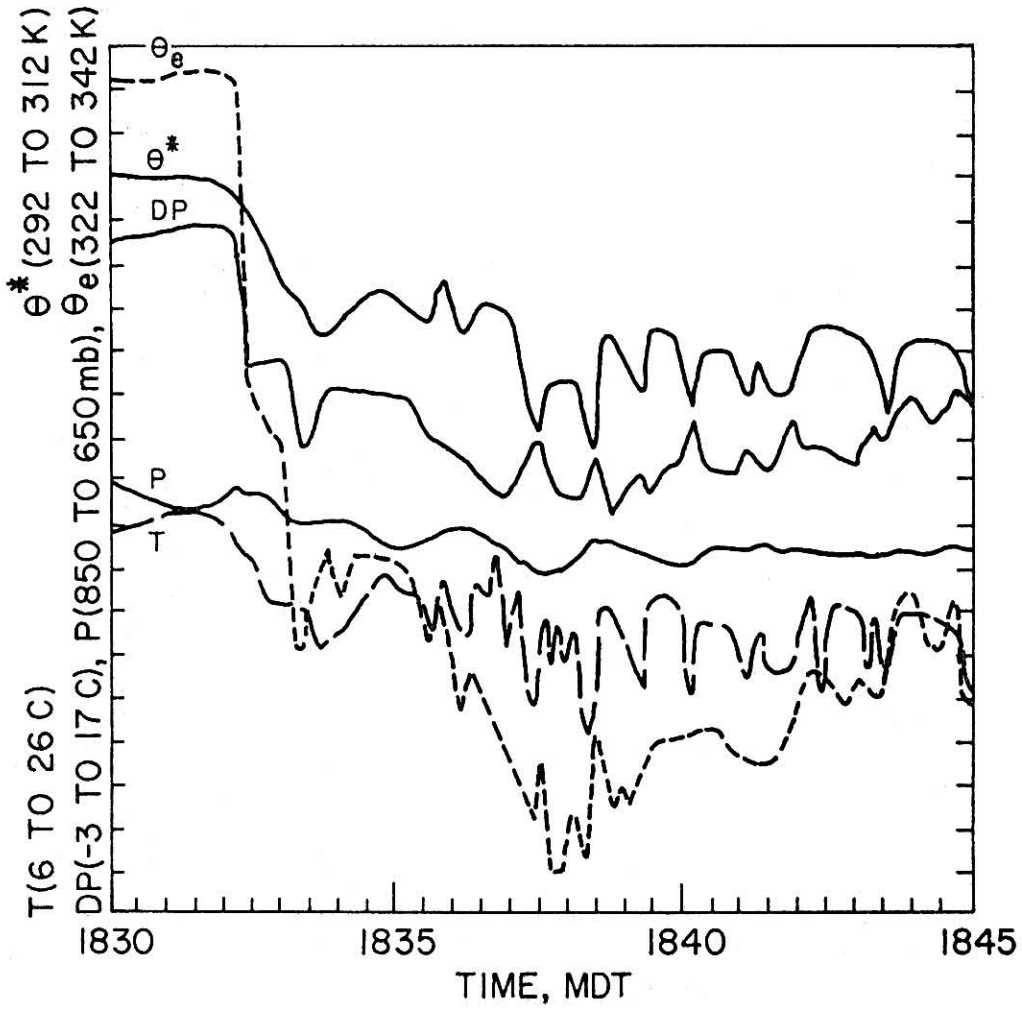

Figure 3.14 Time section of aircraft data (N326D) for the flight segment shown in Figure 3.13. Otherwise, same as Figure 3.8.

occur (as discussed in the previous subsection) these data were interpreted as indicating that a portion of the gust front had its origin near 500 mb. It should also be noted that as a consequence of this strong entrainment, θ^* anomalies across the gust front were as high as 8C (Figure 3.12). Since θ^* is inversely proportional to density, the density gradient between outflow and environment for the storms which produced strong gust fronts is seen to be much greater than that of the northern segment which produced the cloud free vault (refer to Figure 3.10).

3.3 Conclusions

On the basis of the available data, it is speculated that the creation of the cloud free vault along with the lack of severe weather activity on the northern end of the squall line was attributable to minimized entrainment. It is suggested that the orientation of the northern segment of this storm (Figure 3.3) acted to minimize the entrainment in this sector. With entrainment reduced, the outflow failed to gain the density discontinuity required to overcome the momentum of the inflow. Thus, the outflow failed to initiate a gust front and, instead, slowly accumulated between the precipitation and the updraft pedestal.

A further ramification of weak entrainment (and the consequent weak outflow) is in the dynamics of the storm. Lacking strong outflow the updraft would receive little or no dynamical assistance. Such would be the case along the northern end of this squall line. In this case the outflow may, in fact, have interfered with the storm. It appears that

the cloud free vault continued to expand slowly until it eventually separated the inflow from the main echo. At this point, the storm dissipated.

The southern components of the storm, on the other hand, experienced stronger entrainment (because of their orientation to mid-level winds), developed robust outflow and became more severe.

CHAPTER IV

THE CLOUD FREE VAULT: ITS ORIGIN AND IMPORTANCE

4.1 The Origin of the Vault

The storm which forms the basis for this case study was unique in that different elements of the squall line developed to varying degrees of severity under approximately the same environmental conditions giving rise to a cloud free vault in that portion of the squall line which was aligned parallel with the cloud level winds. The availability of comparison data from the other segment of the squall line made it possible to analyze this phenomenon. Had the cloud free vault formed without the attendant severe weather to the south, speculation on its origin may not have been possible.

Synthesis of these data showed:

1. θ_e values from within the cloud free vault were some 12C cooler than the environment ahead of the storm.
2. θ_e values behind the gust fronts of the southern storm components were found to be ∿20C cooler than the pre-storm environment--an 8C greater θ_e depression than found near the vault.
3. This 8C difference is attributable to different rates of entrainment (as discussed in Section 3.2), with the southern components experiencing the strongest intrusion because of their more direct exposure to mid-level wind flow.

4. Density differences between the outflow and the atmosphere ahead of the storm were greater in the southern segment of the storm than in the northern segment as a consequence of these differing entrainment rates.

The cloud free vault is thus postulated to form as a result of inflow air (low in density) passing over a volume of slowly accumulating, weak outflow. Due to the slight vertical bulge on the head of this outflow (e.g., Charba, 1974), the cloud base of the inflow is forced above the LCL (see Figure 4.1).

4.2 The Importance of the Vault

A thunderstorm case study by Miller et al. (1975) had its major inflow located on the upwind side of the storm (with respect to the cloud level winds). The down shear tilted updraft therefore blocked entrainment of dry, mid-level air. Weak outflow and no gust front was noted by the authors. Re-examination of voice notes and photographs showed that this storm also contained a cloud free vault. Both the 22 July 1973 squall line and the 31 July 1973 thunderstorm illustrate the contention that without significant mid-level entrainment, strong gust fronts do not form. The Grover squall line study (and perhaps the study by Miller et al.) further shows that the formation of a cloud free vault is important as an indicator of weak outflow.

A further implication of the Grover squall line study is that when a squall line is oriented parallel to mid-level wind flow, there is reason to expect that the storm will not reach as high a level of

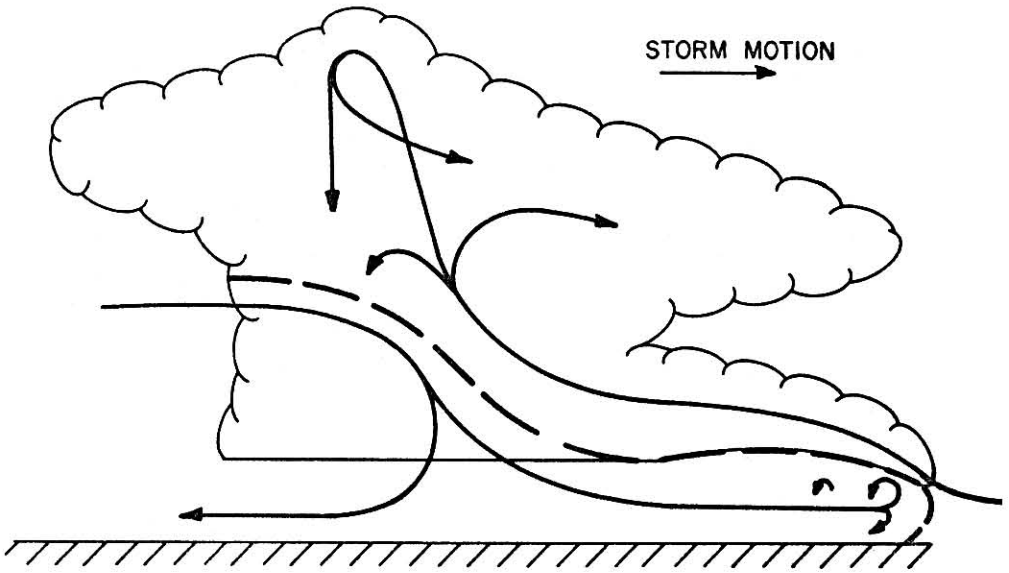

Figure 4.1 Newton's (1966) vertical cross section of a single storm in a squall line modified to show the relationship of the cloud free vault to the principal branches of air circulation as determined from this case study (compare with Figure 1.3).

severity as one oriented more normal to these winds. It could be suggested that the presence of the vault indicates the imminent dissipation of the associated segment of the squall line. This phenomenon has, therefore, a possible short term predictive value with respect to storm severity, especially as applied to gust fronts.

These conclusions may have ramifications to squall line seeding by rocketry. It is apparent that shooting a rocket into the updraft pedestal near the vault would not achieve the desired effect, since this inflow might be extremely shallow. The seeding material would thus not be dispersed into the inflow, but might instead pass into an area of non-convective cloud material above the roof of the cloud free vault.

REFERENCES

Auer, Jr., A. H., D. L. Veal and J. D. Marwitz, 1970: The identification of organized cloud base updrafts. *J. Rech. Atmos.*, 4, 1-5.

Biter, C. J. and C. G. Wade, 1975: Field calibration and intercomparison of aircraft meteorological measurements. NHRE Symposium/ Workshop on Hail, Estes Park, Colorado, September 21-28, 1975.

Browning, K. A., 1962: Cellular structure of convective storms. *Meteor. Mag.*, 91, 341-350.

_____ and R. Donaldson, Jr., 1963: Airflow and structure of a tornadic storm. *J. Atmos. Sci.*, 20(6), 533-545.

_____ and G. B. Foote, 1975: Airflow and hail growth in supercell storms and some implications for hail suppression. *NHRE Tech. Report No. 75*, 75 pp.

_____ and F. Ludlam, 1962: Airflow in convective storms. *Quart. J. Roy. Meteor. Soc.*, 88(376), 117-135.

Byers, H., 1965: *Elements of Cloud Physics*. The University of Chicago Press, Chicago, Illinois, 191 pp.

_____ and R. Braham, Jr., 1948: Thunderstorm structure and circulation. *J. Meteor.*, 5(3), 71-86.

Charba, J., 1974: Application of gravity current model to analysis of squall-line gust front. *Mon. Wea. Rev.*, 102, 140-156.

Endsley, K. and D. Knowlton, 1973: Aircraft data acquisition system for the University of Wyoming research aircraft. *Report No. AR109*, Department of Atmospheric Sciences, University of Wyoming, Laramie, Wyoming, 18 pp.

Friedman, M., 1972: A new radiosonde case: The problem and the solution. *Bull. Amer. Meteor. Soc.*, 53(9), 884-887.

Hess, S. L., 1966: *Introduction to Theoretical Meteorology*. Holt, Rinehart and Winston, New York, New York, 362 pp.

Humphreys, W., 1914: The thunderstorm and its phenomena. *Mon. Wea. Rev.*, 42(6), 348-380.

Lee, H. D. P., 1962: *Aristotle Meteorologica, with an English Translation.* Harvard University Press, Cambridge, Massachusetts, 77, 223-225.

Lenhard, R. W., 1970: Accuracy of radiosonde temperature and pressure-height determination. *Bull. Amer. Meteor. Soc.*, 9, 842-847.

Ludlam, F., 1963: Severe local storms: A review. *Meteor. Mono.*, 5(27), 1-32.

MacCready, P. B., Jr., 1964: Standardization of gustiness values from aircraft. *J. Appl. Meteor.*, 3, 439-449.

Marwitz, J. D., 1972: The structure and motion of severe hailstorms. Part I: Supercell storms. *J. Appl. Meteor.*, 2(1), 165-179.

_____ and E. Berry, 1971: The airflow within the weak echo region of an Alberta hailstorm. *J. Appl. Meteor.*, 10(3), 487-492.

_____, A. J. Chisholm and A. H. Auer, Jr., 1969: The kinematics of severe thunderstorms sheared in the direction of motion. *Proc. 6th Severe Local Storms Conference*, Chicago, Illinois.

Mason, B. J., 1971: *The Physics of Clouds.* Oxford Press, Belfast, Ireland, 671 pp.

Miller, L. J., J. D. Marwitz and J. C. Fankhauser, 1975: Kinematic structure of a Colorado thunderstorm. *Proc. 16th Radar Conference*, Houston, Texas.

National Hail Research Experiment Operations Plan 1973. National Center for Atmospheric Research, Boulder, Colorado, Appendex A.

Newton, C. W., 1966: Circulations in large sheared cumulonimbus. *Tellus*, 18(4), 699-713.

Normand, Sir Charles, 1938: An instability from water vapour. *Quart. J. Roy. Meteor. Soc.*, 64, 47-69.

Ranz, W. E. and W. Marshall, Jr., 1952: Evaporation from drops, Part II. *Chem. Engr. Progress*, 48(3), 173-180.

APPENDIX A

AIRCRAFT INSTRUMENTATION

AIRCRAFT INSTRUMENTATION, N10UW, FROM NHRE (1973)

Parameter Measured	Instrument Type	Manufacturer and Model No.	Combined Performance of Transducer, Signal Conditioning and Recording				
			Range	Accuracy	Time Constant	Precision	Resolution
Heading	Magnetic	King Radio Corp. KPI 550A	0-360°	±1°	1 sec	.36°	.36°
Position Azimuth	VOR	King Radio Corp. KNR 660	0-360°	±1°	1 sec	.36°	.36°
Position Distance	DME (VOR)	King Radio Corp. KDM 700	0-100 mi	.1 mi	1 sec	.1 mi	.1 mi
Altitude	Static Pressure	Rosemount Engr. Co. 1301 A 2A A4AX	0-15 psia	.015 psia	1 sec	.015 psia	.015 psia
IAS		Rosemount Engr. Co. 1301 B 1A D1AX	0-3 psid	.003 psid	1 sec	.003 psid	.003 psid
Dew Point	Peltier Cooled Mirror	Cambridge Sys., Inc. 137-C3	-50°C +50°C	± .5 above 0°C ± 1 below 0°C	1 sec @ ΔT_d<3°	.1°C	.1°C
Liquid Water	Hot Wire LWH	Bacharach Inst. Co.	0-3 gm/m^3	.3 gm/m^3	1 sec	unknown	.003 gm/m^3
Rate of Climb	Calibrated Leak Pressure	Ball Engr. Co. 101-B	±3000 fpm	50 fpm	1 sec	3 fpm	3 fpm
Turbulence	Pressure	Meteorology Res. Inc. 1120	0-10 IT	1 IT	3 sec	.02 IT	.01 IT
Filter Manifold Press.	Pressure	Rosemount Model 831A	0-8 psid	.04 psid	1 sec	.02 psid	.02 psid
Total Air Temperature	Platinum Resistance	Rosemount Engr. Co 510BF9 Bridge Model 102 Probe	+50°C -50°C	1.0°C	1 sec	.1°C	.1°C
Aircraft Manifold Press.	Pressure	Rosemount Model 1331	0-15 psia	.1 psia	1 sec	.1 psia	.1 psia
continued							

Computed Parameters:

1. Aircraft Pitch Angle
2. Aircraft Roll Angle
3. Vertical Wind
4. True Air Speed
5. Potential Temperature
6. Pressure Altitute
7. Indicated Air Speed 8. Vertical Velocity 9. Specific Humidity
10. Equivalent Potential Temperature 11. Static Temperature

Description of Recording System: recording system capabilities: pilot events - 10 positions; meteorologist/copilot events - 10 positions; technician events - 10 positions; aircraft operating events - 36 positions. Additional system control capabilities: telemetry; fault detection system; calibration system; cockpit display; tape stripping; digital data display; course plotting.

AIRCRAFT INSTRUMENTATION, N10UW, FROM NHRE (1973) (continued)

Parameter Measured	Instrument Type	Manufacturer and Model No.	Characteristics of Transducer, Signal Conditioning and Recording				
			Range	Accuracy	Time Constant	Precision	Resolution
Time	Crystal osc.	Dept. Atmos. Res. NA	12 mo.	1 sec	NA	NA	1 sec
Angle of Attack	Syncro	Bendix Corp. 503-26-A2	± 90°	.18°	1 sec	.02°/sec	.02°/sec
Roll Rate	Rate Gyro	Smith Ind., Inc. 401RGS/1	± 20°/sec	.2°/sec	1 sec	.02°/sec	.02°/sec
Pitch Rate	Rate Gyro	Smith Ind., Inc. 401RGS/1	± 20°/sec	.2°/sec	1 sec	.02°/sec	.02°/sec
Vertical Acceleration	Acceleration	Sunstrand Corp. 971-0004-006	+3 -1g	.004g	1 sec	.004g	.004g
Fluorescent Particle Concentrations	Fluorescent Particle Counter	Mee Industries Model 110	0-5000 particles/ liter	NA	1 sec	NA	1 particle/ liter

AIRCRAFT INSTRUMENTATION, N304D & N 306D, FROM NHRE (1973)

Parameter Measured	Instrument Type	Manufacturer and Model No.	Combined Performance of Transducer, Signal Conditioning and Recording				
			Range	Accuracy	Time Constant	Precision	Resolution
Air Temperature	Reverse Flow (Pt. Resistance)	NCAR (in-house)	-70 to +50C	±0.5C	5 sec	±0.1C	0.06C
Total Air Temperature	Platinum Resistance	Rosemount Engr. Model 102E2AL	-70 to +50C	±0.5C	1.5 sec	±0.1C	0.1C
Static Pressure	Variable Capacitance	Rosemount Engr. Model 1301A4BX	0 to 1010 mb	±1.0 mb	0.5 sec	±1 mb	0.5 mb
Airspeed (Dynamic Pressure)	Variable Capacitance	Rosemount Engr. Model 1301D1BX	0 to 200 mb (0 to 360kt)	0.5 mb (approx. 1 kt)	0.5 sec	±.5 mb	.1 mb (approx. .2 kt
Dew Point	Frost Point Hygrometer	Cambridge Systems Model 137-S10A-P	0 to +50C -30 to 0C -50 to -30C	±0.3°C ±0.6°C ±1.1°C (Mfr. specs)	2°C/sec (nominal)	±0.5C	0.1C
Ground Speed	Doppler Radar	Singer General Precision APN-153V	0 to 999 kts	Undetermined	Undetermined	Undetermined	0.24 kt
Drift Angle	Doppler Radar	Singer General Precision APN-153V	+40 to -40 deg	Undetermined	Undetermined	Undetermined	0.1 degree
Magnetic Heading	Gyro Compass	Sperry Model N-1	0 to 360°	±1.0 degree	Undetermined	Undetermined	0.1 degree

Computed Parameters:

1. Static Temperature
2. True Airspeed
3. Horizontal Wind
4. Geographical Position

Description of Recording System: In-house developed hybrid system capable of recording analog and digital inputs serially on magnetic tape. The sampling frequency for each instrument varies in accordance with instrument specifications.

AIRCRAFT INSTRUMENTATION, N326D, FROM NHRE (1973)

Parameter Measured	Instrument Type	Manufacturer and Model No.	Combined Performance of Transducer, Signal Conditioning and Recording				
			Range	Accuracy	Time Constant	Precision	Resolution
Total Air Temperature	Platinum Resistance	Rosemount Engr. Co. 102E2AL	-50 to +50°C	±0.5°C	1.1 sec	±.1°C	0.1°C
Air Temperature	Tungsten Resistance Wire	Built in-house	-100 to +50°C	±1°C	.01 sec	±.3°C	0.03°
Geometric Altitude	Radio Altimeter	Raytheon Mfg. Co. AN/APN-22	0 to 10,000 ft.over land	± 5% of indicated alt	---	---	2.0 ft. at 200 or less
Static Pressure	Variable Cap. Transd.	Rosemount Engr. Co. Model 830BC25	1100 to 300mb	± 1 mb	0.5 sec	±0.5 mb	0.35 mb
Dynamic Press (Air Speed)	Variable Cap. Transd.	Model 831BC2	0-300 kt	± 1 kt	0.5 sec	±0.5 kt	0.2 kt
Dynamic Press (Air Speed)	Strain Gage Press. Transd.	Statham	0-70 mb	2% full scale	0.02 sec	0.7 mb	0.05 mb
Rate of Press. Change	Differential Press. Sensor	Ball Variometer	± 3000 ft/min	---	---	---	---
Dew Point Temperature	Frost Point	Cambridge Model 137-C3	-50° to +50°C	±0.5°C above 0°C ±1°C below 0°C	1 sec @ ΔT_d<3°C	.1°C	.1°C
Ground Speed	Doppler Radar	Singer-General Prec Co., APN-153V	0-999 kt	---	---	---	.25 kt
Drift Angle	Doppler Radar	Singer-General Prec Co., APN-153V	±40°	---	---	---	0.1°
Magnetic Heading	N-1 Compass	Sperry Gyroscope	360°	---	---	---	0.15°
Attack and Slideslip Angles	Non-rotating force-sensing vanes	Lockheed	±8°	0.5°	.03 sec	±0.05°	0.02°
Attack Angle	Rotating Vane	Built in-house	±10°	0.5°	.03 sec	±0.08°	0.03°
continued							

Computed Parameters:

1. Static Temperature
2. True Air Speed
3. Horizontal Wind
4. Vertical Gust Velocities
5. Geographical Position
6. Vertical Acceleration

Description of Recording System: In-house developed hybrid system capable of recording analog and digital inputs serially on magnetic tape. The sampling frequency for each instrument varies in accordance with the instrument specifications.

AIRCRAFT INSTRUMENTATION, N326D, FROM NHRE (1973) (continued)

Parameter Measured	Instrument Type	Manufacturer and Model No.	Combined Performance of Transducer, Signal Conditioning and Recording				
			Range	Accuracy	Time Constant	Precision	Resolution
Airplane Alt; Angles (pitch, roll, azimuth)	Inertial Navigation System	Litton LN-15D	0-360°	0.1°	0.1°	±0.05	0.02°
Airplane Velocity (along all 3 axes)	Inertial Navigation System	Litton LN-15D	---	80 cm/sec	---	±10 cm/sec	0.5 cm/sec
Refractivity	Microwave Refractometer	NOAA/WPL	300 N	not absolute	0.03 sec	1 N	.05 N
IR Radiation termperature	Emersed Thermistor Detector	Barnes Eng. Co. PRT-6	-50 to +50°C 1. No filter 1.8-22μ 2. Filter #1 8.1-13.1μ 3. Filter #2 8.9-12.0μ	0.5°C $\pm .05 \frac{\text{microwatts}}{\text{cm}^2}$ or 2% of full scale, whichever is greater	.003 or .150 sec depending on bandwidth	-----	0.1°C